Revision 1

The origin of extensive Neoarchean high-silica batholiths and the nature of intrusive complements to silicic ignimbrites: insights from the Wyoming batholith, U.S.A.

Davin A. Bagdonas[1*] Carol D. Frost[1#] and C. Mark Fanning[2]

[1]Department of Geology and Geophysics, University of Wyoming, Laramie WY 82071

[2]Research School of Earth Sciences, Australian National University, Canberra, Australia

* E-mail: abags@uwyo.edu, # E-mail: frost@uwyo.edu

Abstract

Extensive intrusions composed entirely of biotite granite are common in Neoarchean cratons. These granites, which have high silica and potassium contents, are not associated with intermediate and mafic phases. One such Neoarchean granite batholith, herein named the Wyoming batholith, extends more than 200 km across central Wyoming in the Granite and the Laramie Mountains. From field characterization, petrology, geochemistry, and Nd isotopic data we establish that the magnesian Wyoming batholith exhibits continental arc chemical and isotopic signatures. It is best interpreted as a large, upper crustal silicic batholith that likely formed when the subducting oceanic plate steepened or foundered, bringing mantle heat and mass to the base of the crust. Similar Cenozoic settings such as the Altiplano-Puna plateau of the Andes and the volcanic provinces of the western United States, host large volumes of silicic ignimbrite. The magma chambers supplying these eruptions are inferred to be silicic but the structural, petrologic, and geochemical details are unknown because the batholiths are not exposed. We suggest that the Wyoming batholith represents an analog for the plutonic complex underlying these ignimbrite systems, and provides an opportunity to examine the shallow magma chamber directly. Our work establishes that aside from more leucocratic margins, the sill-like magma chamber is petrologically and chemically homogeneous, consistent with effective mixing by vertical convection. Nd isotopic variations across the batholith indicate that horizontal homogenization is incomplete, preserving information about the feeder system to the batholith and variations in magma sources. The late Archean Earth may present optimal conditions for the formation of extensive granite batholiths like the Wyoming batholith. By this time the majority of the planet's continental crust had formed, providing the environment in which differentiation, distillation, and assimilation could occur. Moreover, the Neoarchean Earth's relatively high radioactive heat production provided the power to drive these processes.

Keywords: granite, ignimbrite, continental arc, batholith, Archean

Introduction

Continental arc batholiths form from magmas that are relatively oxidized, wet, and cool. These rocks, dominated by granodiorite, are magnesian, calc-alkalic, and metaluminous (Christiansen, 2005; Bachmann and Bergantz, 2008; Frost and Frost, 2014). Small volumes of true granite are components of continental arc batholiths. These granite bodies tend to be younger than the granodiorites, consistent with their origin by differentiation. If the granites are end-products of differentiation of a basaltic parent, then they represent the less than 5% of the volume of original magma. Even if the starting material is granodiorite and differentiation is accompanied by crustal assimilation, the volume of less silicic cumulates will be 2-3 times greater than the volume of granite produced (Lee and Morton, 2015). As a result, it is not surprising that granites make up a relatively modest proportion of continental arc batholiths.

In contrast, intrusions composed exclusively of granite are a notable feature of the Neoarchean geologic record. Biotite and two-mica granites are a common component of every Archean craton, and are the second most widespread lithology in Neoarchean terranes after the tonalite-trondhjemite-granodiorite association (Laurent et al., 2014). These granites, which have silica contents of 70-76%

SiO_2, are not associated with intermediate and mafic phases, they are calc-alkalic to alkali-calcic, peraluminous, and high-K (Laurent et al., 2014). The granites are typically undeformed, extensive, and are widely distributed throughout the host craton. Most petrogenetic models for the formation of Neoarchean potassic granites call upon partial melting of older tonalite-trondhjemite-granodiorite crust or metasedimentary rocks (Moyen, 2011; Jaguin et al., 2012). Even if the magma sources lie dominantly within the crust, the production of such large volumes of granite across a broad area seems to require a large power input from the mantle.

This study documents a large batholith composed entirely of magnesian biotite granite in west-central Wyoming. It is petrologically indistinguishable from a late-stage granite pluton within a contemporary Neoarchean continental arc composite batholith exposed in the neighboring Wind River Range. This granite batholith, here named the Wyoming batholith, is exposed in Laramide basement-involved uplifts that extend 200 km from east to west. It is everywhere composed of undeformed biotite granite, even though outcrops expose varying structural levels. We investigate its petrogenesis and its potential similarity to the granitic batholiths that are inferred to underlie large silicic ignimbrite provinces.

Geologic setting

The Neoarchean magmatic rocks of central Wyoming compose part of the Wyoming province, an Archean craton that extends across most of Wyoming and parts of Montana, Idaho, Utah, and South Dakota (Fig. 1). Today rocks of the Archean Wyoming province are exposed in the cores of basement-involved, Laramide uplifts. The craton is composed of several sub-provinces (Fig. 1). The Montana metasedimentary province lies in the northwest part of the craton and is composed of Neoarchean quartzite, pelite and carbonate rocks structurally intercalated with Paleoarchean quartzofeldspathic gneiss (Mogk et al., 1988, 1992; Mueller et al., 1993, 2004; Mueller and Frost, 2006). The Beartooth-Bighorn magmatic zone (BBMZ) is dominated by ~2.8 Ga tonalites and granodiorites, although rocks as old as 3.5 Ga and detrital zircons as old as 4.0 Ga have been identified (Mueller et al., 1996; 1998, Frost and Fanning, 2006). The BBMZ is characterized by radiogenic whole rock and feldspar $^{207}Pb/^{204}Pb$ ratios and Nd model ages up to 4.0 Ga (Mueller and Frost, 2006). The Wyoming province grew southward (present-day coordinates) through accretion of terranes between 2.68 and 2.65 Ga. Some of these southern accreted terranes are juvenile, and others contain pre-existing continental crust (Mueller and Frost, 2006; Souders and Frost, 2006; Chamberlain et al., 2003).

Neoarchean granitic rocks dominate the Archean exposures of central Wyoming along the boundary of the BBMZ with the southern accreted terranes (Fig. 1, 2). The 2.63 Ga Louis Lake batholith occupies the southern half of the Wind River Range (Fig. 2; Stuckless et al., 1985; Frost et al., 1998). This batholith, which is exposed over an area >1,600 km^2, is composed of a suite of undeformed, calc-alkalic diorites, granodiorites, and granites. It is intruded by a biotite granite body known as the Bears Ears pluton, which varies from equigranular to porphyritic. This composite batholith was derived from magmas composed of varying proportions of crustal and mantle sources, and has been interpreted as a continental magmatic arc complex (Frost et al., 1998).

East of the Wind River Range, Precambrian exposures in the Granite Mountains, Shirley Mountains, and Laramie Mountains consist exclusively of monotonous, undeformed, biotite granite despite Laramide and younger basement-involved faulting that exposes varying structural depths. U-Pb geochronology suggests that the granites are ~2.62-2.63 Ga (Ludwig and Stuckless, 1978; Wall, 2004; Bagdonas, 2014). Precambrian exposures are extensive in the Laramie Mountains, but Tertiary sedimentary rocks cover much of the Precambrian basement to the west in the Shirley Basin and in the vicinity of the Granite Mountains. Nevertheless, structural and geophysical evidence is consistent with the hypothesis that biotite granite extends at least 200 km east-west across the area (present coordinates). There are no major faults between the Granite and Laramie Mountains, and the top of the Precambrian basement between the two mountain ranges is relatively shallow (~2 km; Robbins and Grow, 1992). Complete Bouger gravity anomaly and isostatic residual anomaly maps show similar anomalies in both mountain ranges, and a smooth gradient to values 15-20 mgals lower in the intervening basin is interpreted to reflect low-density basin fill. These characteristics have been interpreted to suggest that felsic basement extends from the Granite Mountains to the Laramie Mountains (Robbins and Grow, 1992). If the entire area from the Granite Mountains to the Laramie Mountains is underlain by biotite granite, then it occupies an area of more than 6,900 km^2. Because it appears so extensive, we refer to this Neoarchean granite as the Wyoming batholith.

Few contacts of the Wyoming batholith with its country rocks are exposed. In the eastern Granite Mountains the northern margin of the Wyoming batholith intrudes 3.30-3.45 Ga gneisses (McLaughlin et al., 2013; Frost et al., 2015). Both the Neoarchean granite and Paleoproterozoic gneisses are silicified and epidotized along the contact. In addition, the contacts are commonly occupied by younger diabase dikes. The southern contact of the Wyoming batholith in the Granite Mountains is fault-bounded. Pliocene motion on the southern Granite Mountains fault down-dropped the Granite Mountains by a minimum of 600 meters (Love, 1970). No contacts with older rocks are exposed in the Shirley Mountains. In the Laramie Mountains, the northern and southern contacts are exposed but the eastern and western margins are covered by Cenozoic sedimentary rocks. The northern and southeastern contacts of the granite are gradational and marked by development of biotite foliation against the host gneisses. The southwestern contact is fault-bounded (Condie, 1969).

The Wyoming batholith

Previous studies have described portions of the Wyoming batholith. The Granite Mountains granites were investigated by the U.S Geological Survey (e.g., Peterman and Hildreth, 1978; Stuckless et al., 1977; Stuckless and Miesch, 1981) and were the subject of theses by Langstaff (1995), Wall (2004), and Meredith (2005). The Bear Mountain granite, an exposure of the Wyoming batholith near the southern Granite Mountains fault, was described by Bowers and Chamberlain (2006). Condie (1969) reported on the mineralogy and petrology of the Laramie Mountains granites. For this study, the lead author undertook extensive field observations across the entire Wyoming batholith, including the first systematic study of the granites in the Shirley Mountains (McLaughlin et al., 2013; Bagdonas, 2014).

Field relations and petrography

Very little petrographic diversity exists within the Wyoming batholith, although magmatic fabrics are observed particularly adjacent to country rock. Two main lithologic units are identified throughout the batholith on the basis of field observations and petrography: biotite granite and leucocratic banded granite. Both of these units may be hydrothermally altered, as described by Ludwig and Stuckless (1978). Where altered, the granites form blocky outcrops that are more resistant to weathering than the unaltered rocks.

Leucocratic banded granite appears to be more common along batholith margins. It is present along the northern contact with older country rocks in the northwestern Granite Mountains where banding in the granite parallels the contact. Leucocratic banded granite may also form near the roof of the batholith, as suggested by its location on the summit of Lankin Dome (Fig. 3a). Contacts with biotite granite are abrupt to gradational, and are commonly scalloped to feathery (Fig. 3b,c). Leucocratic banded granite tends to be coarse-grained along these contacts. In other places, leucocratic banded granite is incorporated within biotite granite. On an inselberg near Sweetwater station in the Granite Mountains leucocratic banded granite appears both on the summit and as folded enclaves and lenses within biotite granite (Fig. 3d). We attribute these relationships to entrainment of solidified banded granite from batholith margins into more melt-rich biotite granite crystal mush.

Biotite granite. Biotite granite is the dominant rock type of the Wyoming batholith, occupying approximately 90% of outcrop. Most is medium- to coarse-grained, although fine-grained varieties were observed in the Shirley and Laramie Mountains and slightly porphyritic biotite granite was found in places in the Laramie Mountains. Biotite granite is composed of 30-40% microcline, 25-35% quartz, 25-35% plagioclase (An_5-An_{30}), and 1-7% biotite. Accessory minerals include epidote, titanite, magnetite, zircon, and apatite (Fig. 4a-c). Trace amounts of muscovite are present in some localities. Biotite granite generally is homogeneous, exhibits weak to no fabric, and lacks mafic enclaves. Foliation in biotite granite is magmatic, and is marked by aligned plagioclase and biotite. No post-magmatic deformation is evident in these rocks.

Leucocratic banded granite. Leucocratic banded granite comprises approximately 10% of outcrops and is present across the Wyoming batholith. It is characterized by millimeter- to decameter-scale compositional banding, typically defined by aligned biotite and most likely formed due to magmatic flow. Leucocratic banded granite is composed of 35-40% quartz, 20-35% microcline, 20-30% plagioclase, 0-5% biotite and 0-5% magnetite. In some localities it contains sparse potassium feldspar phenocrysts. Accessory minerals include epidote, titanite, zircon and apatite. Magnetite ranges from mm- to cm-diameter and appears to form at the expense of biotite (Fig. 4d-f).

Geochronology

Past efforts to date Wyoming batholith granites have established that uranium concentrations of Wyoming batholith zircon are high and alpha-recoil damage has led to considerable open-system behavior (Ludwig and Stuckless, 1978). For this study, U-Pb isotopic data on zircon from three Wyoming batholith samples were obtained using SHRIMP RG at the Australian National University. Zircon grains mounted in epoxy together with chips of the Temora reference zircons (Black et al., 2003) and polished. Cathodoluminescence (CL) Scanning Electron Microscope (SEM) images were taken for all zircons. The U-Th-Pb analyses were performed following procedures given in Williams (1998, and references therein). Temora reference zircon grains were analyzed after every three unknown analyses. The data were reduced using the SQUID Excel Macro of Ludwig (2001). The Pb/U ratios were normalized relative to a value of 0.0668 for the Temora reference zircon, equivalent to an age of 417 Ma (Black et al., 2003). Uncertainties given for individual analyses (ratios and ages) are at the one sigma level with correction for common Pb made using the measured $^{207}Pb/^{206}Pb$ ratios. Concordia plots, linear discordia regression fits and weighted mean $^{207}Pb/^{206}Pb$ age calculations were carried out using either ISOPLOT or ISOPLOT/EX (Ludwig, 2003). Weighted mean $^{207}Pb/^{206}Pb$ ages are calculated and uncertainties reported at the 95% confidence level. 53 analyses yielded uranium contents of 279-4984 ppm and discordant U-Pb compositions (Supplementary Tables S1-3). Data interpretation below focuses on those grains with the lowest uranium concentrations and most concordant U-Pb isotopic compositions. The CL images for all samples show either simple igneous internal structures, mostly oscillatory zoning, or are dominated by metamict areas, interpreted as having replaced the primary igneous zoning.

Leucocratic banded granite (10LD2). Sample 10LD2 was collected from the summit of Lankin Dome, a sample of leucocratic banded granite with very little feldspar and biotite alteration. A single morphology of euhedral zircon grains yielded uranium concentrations from ~280-3115 ppm. Data from three high uranium zircons that were >50% discordant were not considered. A 7-point regression of the remaining analyses yielded an imprecise upper concordia intercept of 2628 ± 21 Ma (MSWD = 4.7). The single concordant analysis gave a $^{207}Pb/^{206}Pb$ age of 2627 ± 3 Ma (1σ), which we interpret as the best estimate of the magmatic age for this sample (Figure 5a).

Biotite granite sample 11SMG1. This sample also yielded euhedral zircon, with some grains coarser than ~200μm in length and others around 100μm; both smaller and larger grains yielded indistinguishable dates. Uranium contents range from ~450 to ~4985 ppm, and most areas analyzed have lost radiogenic Pb; up to ~50% discordant. A cluster of 5 analyses of zircon with U < 600 ppm and from ≤4% discordant define an upper intercept age of 2626 +16/-9 Ma (MSWD = 0.60). These analyses yield a mean weighted $^{207}Pb/^{206}Pb$ age of 2623 ± 4.3 Ma (MSWD = 1.02), which we interpret as the best estimate of the crystallization age (Fig 5b). A sixth low-U zircon gave a $^{207}Pb/^{206}Pb$ age of ~2715 Ma, which we interpret as reflecting an inherited component.

Hydrothermally altered biotite granite sample 11SMG2. This sample of biotite granite exhibits strong hydrothermal alteration fabrics, with complete replacement of feldspars by sericite, biotite by chlorite and epidote, and significant quartz sub-grain development. Uranium contents of zircon are high, up to 5615 ppm, and most analyses are strongly discordant. The two grains with the lowest uranium contents yielded $^{207}Pb/^{206}Pb$ ages of 2624 ± 4 Ma (-1% discordant) and 2614 ±7 Ma (5% discordant; Fig 5c). We interpret the more concordant analysis as the best estimate of the crystallization age.

These results suggest that the age of the Wyoming batholith is approximately 2625 Ma, similar to unpublished dates obtained by other workers (see Bagdonas, 2014 for a summary). The Wyoming batholith ages reported here are comparable to dates obtained for the Bears Ears pluton in the Wind River Range of 2620 ± 4 Ma (Wall, 2004) and a granitic dike in the northern Wind River Range of 2618.9 ± 1.5 Ma (Frost et al., 1998). The Wyoming batholith appears to be contemporaneous to slightly younger than the Louis Lake batholith of the Wind River Range, which has been dated at 2629.2 ± 2.8 Ma and 2629.5 ± 1.5 Ma (Frost et al., 1998).

Geochemistry

Twenty Wyoming batholith samples were analyzed by ICP-AES for major and minor element concentrations and by ICP-MS for rare earth element abundances by ALS Minerals, Ltd. (Table 1). These data, combined with analyses from the literature, indicate that the Wyoming batholith is uniformly high in silica (70 to 77% SiO_2; Table 1; Condie, 1969; Stuckless and Peterman, 1977; Stuckless and Miesch, 1981; Wall, 2004; Meredith, 2005). The granites are mainly magnesian, calc-alkalic to alkali-calcic, and peraluminous (Fig. 6). There is no variation in major element composition related to location within the batholith, although the range in aluminum saturation index is greater among samples from the Laramie Mountains than elsewhere in the batholith. The Bears Ears pluton samples plot within the fields defined by Wyoming batholith samples. By contrast, samples of the Louis Lake batholith exhibit a wide range in silica (52-76% SiO_2). Like the Wyoming batholith, the Louis Lake batholith is magnesian. However, Louis Lake batholith samples are mostly calc-alkalic and metaluminous (Frost et al., 1998; Frost et al., 2000; Stuckless et al., 1985; Stuckless, 1989).

Variation diagrams of K_2O, Rb, Sr, and Eu versus SiO_2 (Fig. 7) show elevated concentrations of incompatible elements K_2O and Rb in Wyoming batholith samples and Louis Lake batholith samples with SiO_2 > 70%, relative to the mafic to intermediate rocks of the Louis Lake batholith. These characteristics are consistent with late crystallization of biotite and potassium feldspar. By contrast, elements compatible in plagioclase, such as Sr and Eu, are lower in the high-silica rocks than in the Louis Lake batholith. Elements compatible in hornblende, such as Nb and Y, are higher in the quartz diorite and granodiorite Louis Lake batholith samples than in the Wyoming batholith and Bears Ears granites. Both batholiths plot mainly in the volcanic arc granite field of Pearce et al. (1984; Fig. 8), though Louis Lake batholith samples with cumulate hornblende, and accordingly higher Nb and Y, extend beyond.

Rare earth element (REE) patterns for the Wyoming batholith exhibit some variability (Fig. 9). Biotite granites from the Granite Mountains have uniform, LREE-enriched and HREE-depleted patterns with negative Eu anomalies whereas banded granite has flatter and higher HREE contents (Fig. 9a). Some samples from the Shirley Mountains lack Eu anomalies, and one sample from the Laramie Mountains has low LREE and a slight positive Eu anomaly (Fig. 9b, c). These variations are interpreted to reflect different proportions of cumulate feldspar, zircon and other REE-bearing accessory minerals in the samples. The REE patterns of hornblende-bearing Louis Lake batholith samples are less HREE-depleted than Wyoming batholith samples (Fig. 9d). The Eu anomaly in Louis Lake batholith samples varies from negative to slightly positive, consistent with differentiation by fractionation (Stuckless et al., 1989; Frost et al., 1998). REE patterns of Bears Ears samples fall within the field defined by Wyoming batholith samples, and variations likely reflect cumulate processes (Fig. 9d).

Nd isotopic compositions

Sm and Nd were isolated from homogenized powders of 17 Wyoming batholith samples using the methods described in Frost et al. (2006) and were analyzed at the University of Wyoming on a Neptune MC-ICP-MS. Samples were normalized to $^{146}Nd/^{144}Nd$ = 0.7219. La Jolla Nd analyzed after every five unknowns gave $^{143}Nd/^{144}Nd$ = 0.51185 ± 0.00001 (2 standard deviations). These data, together with analyses reported by Frost et al. (2006), Fruchey (2002), Wall (2004), and Meredith (2005), show that initial Nd isotopic compositions of the Wyoming batholith vary considerably from +1.9 to -7.8. They mostly overlap data from the Louis Lake batholith and Bears Ears pluton but extend to more negative initial ε_{Nd} (Fig. 10). Nd isotopic compositions correlate with location: in general, samples from the Shirley and Laramie Mountains have less radiogenic initial ratios than samples from the Granite Mountains and Bears Ears pluton (Fig. 11). This suggests that despite the uniformly high SiO_2 of Wyoming batholith samples and their overall geochemical similarity, they do not share a single magma source or common proportions of magma sources.

Although it is not possible to know the Nd isotopic composition of potential magma sources at depth in the Wyoming craton, the Nd isotopic composition has been established for various Archean country rocks that are exposed on the surface today. Country rocks to the Wyoming batholith in the Granite Mountains are composed of 3.3-3.4 Ga gneisses (Fruchey, 2002; Frost et al., 2015). At 2625 Ma, these gneisses had ε_{Nd} values of -9 to -14. Evolved quartzite and pelitic rocks deposited on this basement had slightly more radiogenic ε_{Nd} values at 2625 Ma of between -5 and -4 (Fruchey, 2002), and juvenile metasedimentary rocks accreted to the Wyoming province at approximately 2.67 Ga had

ε_{Nd} values from 1 to +4 (Frost et al., 2006). The wide variation in proportions of juvenile crust or mantle and crust incorporated into Wyoming batholith magmas indicated by the range in initial ε_{Nd} can be quantified by the Neodymium Crustal Index (NCI; DePaolo et al., 1992). Assuming a juvenile end member with ε_{Nd} of +4 and a Paleoarchean crustal source of -12, the proportion of Nd from crustal sources varies from 13 to 73% with an average of 39% (n = 33). The crustal assimilant is likely to have been felsic for two reasons. First, the older Archean crust, where exposed, is dominated by granite, granodiorite, and trondhjemite (McLaughlin et al., 2013; Frost et al., 2015). Second, if the crustal assimilant was of a strongly contrasting composition then a correlation should exist between amount of assimilation and geochemical composition of the Wyoming batholith granite.

The 2630 Ma Louis Lake batholith, which ascended through the crust in the same area where the Bears Ears was later emplaced, also exhibits a range of initial ε_{Nd} (-2.1 to +3.5; Fig. 10). This more restricted range in initial ε_{Nd} compared to the Wyoming batholith is indicative of a lower proportion older crustal sources in the Louis Lake batholith (NCI = 20-37%; n = 11) (Frost et al., 1998). The initial ε_{Nd} of the Bears Ears and the western part of the Granite Mountains overlap those of the Louis Lake batholith. Nd isotopic data permit that the Bears Ears pluton and Wyoming batholith in the Granite Mountains formed either from Louis Lake residual magmas, or from similar proportions of the same sources. In either case, Nd isotopic systematics require that the Wyoming batholith granite farther to the east in the Shirley and Laramie Mountains must have incorporated a larger proportion of older continental crust (Fig. 10, 11).

Discussion

Extent of the Wyoming Batholith

This study has identified a large 2625 Ma biotite granite batholith that extends east-west at least 200 km across the Laramie, Shirley, and Granites Mountains of central Wyoming. In addition, we have shown that the Bears Ears pluton of the Wind River Range is petrographically, temporally, and chemically similar to the Wyoming batholith, and that together these biotite granites dominate a large area of the exposed Archean crust (Fig. 2). It is possible that the Wyoming batholith intrusive event is even more extensive than defined here. For example, it is unclear whether the Prospect Mountain granite of the southwestern Wind River Range is part of the Louis Lake or the Wyoming batholith: Sutherland and Luhr (2011) describe biotite granite that we have confirmed is petrographically similar to the Wyoming batholith. Another possible part of the batholith lies in the Lewiston district at the southeastern end of the Wind River Range, where the granite exposed there is unstudied. It has been assumed to belong with the Louis Lake batholith and Bears Ears pluton, but may equally belong to the Wyoming batholith. Smaller outcrops of ~2.6 Ga granite are also present within the Owl Creek Mountains and on Casper Mountain at the northern end of the Laramie Mountains (Fig 2). In places these granites are garnet-bearing, and their relationship to the Wyoming batholith is uncertain. Even if none of these granites should be considered part of the Wyoming batholith, it remains a large body of true granite, dwarfing the size of the neighboring, roughly contemporary Louis Lake continental arc batholith to the west.

Petrogenesis of the Wyoming batholith

Silica-rich granite is found in many tectonic environments, from extensional regimes and orogenic margins to continental collision zones. Even though their mineralogies are similar, silica-rich granites retain in their major and trace element geochemical compositions evidence of their petrogenesis (Frost et al., 2016). Large volumes of magnesian granite commonly form by differentiation, usually accompanied by some degree of crustal assimilation (Bachmann and Bergantz, 2008). Two tectonic settings are most likely to the generate magnesian, calc-alkalic to alkali-calcic granite of the Wyoming batholith. The first, a magmatic arc batholith setting, is suggested by the spatial and temporal association of the Wyoming batholith with the Louis Lake continental arc batholith. In this model, the biotite granite of the Wyoming batholith is part of an incrementally assembled composite batholith that also is composed of large volumes of granodiorite and more mafic rocks. The second, a large, shallow silicic system related to a continental arc, is suggested by the abundance of granite and lack of more mafic components. In this model, changes in subduction dynamics allow for a pulse of mantle heat to power melting and the formation of a large silicic magmatic system in the upper crust. Each of these is evaluated in more detail below.

A continental arc batholith? Though dominated by granodiorite, continental arc batholiths also contain true granite (Bateman and Chappell, 1979; Lee et al., 2007). These granites are thought to form by fractional crystallization, and commonly also involve crustal assimilation (e.g., Ague and Brimhall, 1988; Putirka et al., 2014). Such a process may have formed the Bears Ears granite from residual magmas of the Louis Lake continental arc batholith. Geochemically, the Bears Ears pluton samples lie at the high-silica end of Louis Lake batholith differentiation trends. Bears Ears pluton initial ε_{Nd} values are within the range of Louis Lake samples, permitting formation of the Bears Ears granite from Louis Lake granodiorite by differentiation alone. In the field, contacts between the Bears Ears pluton and Louis Lake granodiorites are complex. They are gradational in places, but in others the Bears Ears has intruded the granodiorites. Taken together, all observations are consistent with the crystallization of the Bears Ears granite at the top of the Louis Lake batholith in the latter stages of its development.

The similarities in petrology, age, and geochemistry could suggest that the Wyoming batholith, like the Bears Ears pluton, is also related to a continental arc magmatic system. A difficulty with a continental arc model is the sheer quantity of granite exposed in the Wyoming batholith. To form granite magma by differentiation of a basalt parent requires approximately 95% of the original melt volume to have crystallized (Lee and Morton, 2015). However, none of these voluminous mafic components of such a magmatic system is evident in the Wyoming batholith, which is composed solely of true granite. One possibility is that the structural level of exposure of the Wyoming batholith is higher than the Louis Lake batholith in the Wind River Mountains, such that only the granitic top of the continental arc batholith appears at the erosional surface. Current topographic relief is approximately 1.3 km, and Laramide and Cenozoic faulting has exposed the Wyoming batholith to a minimum of 0.75 km additional structural relief. Yet no other rock types are exposed, even in the deepest sections. Although possible, it seems unlikely that faulting would have brought *none* of the more voluminous, more mafic components of the continental arc batholith to the surface in the Granite, Shirley, and Laramie Mountains as it did in the Wind River Range.

Plutonic equivalent of silicic ignimbrites? Alternatively, the Wyoming batholith may represent the plutonic record of a large rhyolitic system associated with a continental arc. A possible analog system is preserved in the western United States, where large volumes of silicic, high-K ignimbrites formed during the middle Cenozoic. The 35-27 Ma Southern Rocky Mountain volcanic field (SRMVF) of Colorado and northern New Mexico erupted voluminous silicic ignimbrites. The field is composed of dominantly dacitic volcanic tuffs originating from a number of different calderas along with several small, subvolcanic plutons (Lipman, 2007; Lipman and Bachmann, 2015). Farther to the west, the 36-18 Ma southern Great Basin ignimbrite province in Nevada and Utah is dominated by dacites that share a volcanic arc chemical signature with the continental arc rocks to the west (Best et al., 2013a). These volcanic rocks were deposited on a high plateau in an area of orogenically thickened crust known as the Great Basin altiplano (Best et al., 2009). Magmatism is thought to have resulted from progressive steepening of the subducting oceanic Farallon plate (Best et al., 2013a). As the slab rolled back, basaltic parental magmas to the ignimbrites formed by partial melting in the lithospheric mantle and asthenosphere (Christiansen and Best, 2014). Throughout the western United

States, Cenozoic episodes of increased magma production and large ignimbrite eruptions appear to coincide with a regional transition from low-angle subduction to an extensional regime (Lipman, 2007). The Neogene Altiplano-Puna plateau represents a second example of a continental arc setting that yielded voluminous silicic ignimbrites (de Silva and Gosnold, 2007). The thick crust of the Altiplano-Puna plateau in the central Andes formed during a period of flat slab subduction. Steepening of the slab in mid-Miocene time introduced mantle heat and partial melt at the base of the crust, leading to a flare-up in ignimbrite activity (Kay et al., 1999).

In both the western United States and the Altiplano-Puna plateau, the ignimbrites are inferred to be surface manifestations of the formation of large silicic batholiths at depth (Best et al., 2013b; de Silva and Gosnold, 2007; Lipman, 2007), although the plutonic underpinnings of these ignimbrites are not exposed in the Andes and Great Basin, and only small subcaldera intrusions are present in the Southern Rocky Mountain field. However, in the Andes an extensive low-velocity zone has been imaged and interpreted as the sub-volcanic plutonic complex. This shallow low-velocity zone is approximately 200 km in diameter and 11 km thick. The uppermost parts of this zone are suggested to be composed of shallow silicic magma bodies that feed the ignimbrite eruptions (Ward et al., 2014). Similarly, geophysical anomalies in the Southern Rocky Mountain volcanic field may image underlying shallow batholiths of similar dimension (Lipman and Bachmann, 2015).

One potential difficulty with the model of the Wyoming batholith as an intrusive complement to silcic ignimbrites is compositional: most ignimbrites in these settings are crystal-rich dacites, less siliceous than the Wyoming batholith granites. However, crystal-poor ignimbrites tend to be rhyolitic. For example, the second-largest ash-flow sheet in the SRMVF, the Carpenter Ridge tuff, is composed of a basal, crystal-poor densely welded rhyolite with 77-78% SiO_2 (Bachmann et al., 2014). Although the most voluminous SRMVF eruption, the Fish Canyon crystal-rich tuff, is dacitic at around 68% SiO_2, the glass in the tuff has much higher silica, from 76.5-78% SiO_2 (Bachmann et al., 2002). Farther west in the Great Basin, glass within Cottonwood Wash tuff is rhyolitic (Ross et al., 2015) and the crystal-poor, glass-rich portions of the Lund tuff extend into the low-silica rhyolite field (Maughan et al., 2002). These observations have led to the hypothesis that crystal-rich monotonous intermediates represent erupted mush, and that liquid segregated from this mush is the source of high-silica rhyolites (Charlier et al., 2007).

Similar compositional relationships have been documented from the central Andes. For example, the Pliocene La Pacana caldera system on the Altiplano-Puna plateau includes two, large-volume ignimbrites. The older Toconao unit is crystal-poor and rhyolitic (76-77% SiO_2) whereas the younger Atana ignimbrite is crystal rich and dacitic (SiO_2 – 66-70%) but contains glass that is rhyolitic (Lindsay et al., 2001). Another example is provided by ignimbrites from the Cerro Galán caldera on the eastern edge of the Puna plateau (Folkes et al., 2011). Pumice clasts separated from ignimbrite, which are interpreted as erupted crystal mushes, are composed of matrix glass, plagioclase, biotite, and quartz, with lesser amounts of hornblende, sanadine, oxides, and accessory phases. Pumice clasts are rhyodacites, with SiO_2 of most samples between 68.5 and 70.5%. Matrix glass has higher silica, up to 81%, indicating that interstitial liquid was highly evolved (Folkes et al., 2011). Al-in-hornblende barometry suggests that crystals formed in magma chambers at both intermediate (14-18 km) and shallow (6-10 km) depths. This finding is consistent with other workers who have described a model with multiple levels of magma accumulation (e.g., de Silva et al., 2006; de Silva and Gosnold, 2007; Kay et al., 2010). The lowest level is at the base of the crust where mantle melts pond, induce lower crustal melting, and differentiate to produce intermediate magmas. These intermediate magmas rise to a mid-crustal level and fractionate further. Finally, the evolved melts ascend to shallow levels to form silicic sills that feed eruptions. A sill-like magma chamber geometry impedes sidewall crystallization and allows buoyant rhyolitic melt to segregate at the top of the chamber (De Silva and Wolff, 1995; Christiansen, 2005; Bachmann and Bergantz, 2008). The bulk of the magma chamber is composed of silicic cumulates and trapped rhyolitic liquid (Lee and Morton, 2015).

In this model, the Wyoming batholith represents an exposed example of a solidified, shallow silicic magma body that may have fed voluminous felsic ignimbrites like those that blanket the Great Basin and Altiplano-Puna plateau. The ~200 km extent of the Wyoming batholith supports this interpretation: it is comparable to the inferred size of the plutonic complexes supplying large volume silicic ignimbrites. The size of the batholith supplying the Altiplano-Puna ignimbrites is inferred from the extent of a low velocity zone at depths of 4-25 km below sea level. Seismic images of the Altiplano-Puna crust by Ward et al. (2014) determined that this low velocity zone, known as the Altiplano-Puna magma body, exceeds 200 km in diameter. Lipman and Bachmann (2015) interpret two large negative gravity anomalies along the axis of the SRMVF image subvolcanic batholiths, each approximately 100 km in diameter. The size of the batholith supplying the Great Basin ignimbrites is less well-known. If the locations of calderas are interpreted to encompass the minimum size of the batholith beneath, and if corrections are made for subsequent Basin and Range extension (40-50% in this area; Best et al., 2013b), then it appears that the batholith (or batholiths) beneath the Great Basin altiplano were also approximately ~200 km in diameter.

Lacking samples of the batholiths that supplied the Cenozoic ignimbrites it is not possible to ascertain that the compositions of those plutonic rocks are equivalent to the Wyoming batholith. However, inferences can be made by comparing the composition of the Wyoming batholith to ignimbrites erupted from systems inboard of continental magmatic arcs. Ignimbrites from both the Altiplano-Puna and western USA ignimbrites fields are dominated by crystal-rich dacite and rhyodacite. In both locations, the volcanic systems also erupted high-K rhyolite ignimbrites, though these are volumetrically minor (De Silva and Gosnold, 2007; Best et al., 2013b). And in both areas, glass compositions identify the presence of rhyolitic liquid at depth. The ignimbrite compositions encompass those of the Wyoming batholith granites. To illustrate, Figure 12 compares Wyoming batholith granites to the ignimbrites of Cerro Galán, which produced magmas with nearly identical geochemistries for over 3.5 Ma (Folkes et al., 2011). The K_2O and silica contents of the Cerro Galán rhyodacite pumice clasts are slightly lower than the Wyoming batholith, and analyses of rhyolite glass are overlapping to higher (Fig. 12). We conclude that if it had erupted, the Wyoming batholith could conceivably have produced a similar spectrum of ignimbrite compositions by eruption of segregated rhyolitic liquid and of dacitic crystal mush.

Implications

We suggest that the Wyoming batholith is best interpreted as an upper-crustal silicic plutonic system generated in a continental arc setting (Fig. 13). The plutonic roots of the continental arc are represented by the 2.63 Ga Louis Lake batholith, a magnesian, calc-alkalic composite arc exposed in the Wind River Range. The Louis Lake batholith intruded older Archean crust and juvenile graywackes interpreted as an accretionary prism (Frost et al., 1998; Frost et al., 2006). The Louis Lake batholith crystallized at between 3 and 6 kb (10 to 20 km; Frost et al., 2000). It is a composite batholith composed of a wide range of rock types from gabbro to granite, and the youngest intrusion, the Bears Ears pluton, is geochemically indistinguishable from the Wyoming batholith.

The Wyoming batholith is a large body of true granite. Except for slightly more leucocratic margins, it exhibits no apparent zoning or heterogeneity despite being exposed at different structural levels. These characteristics are consistent with a sill-shaped magma chamber, where the rise of buoyant evolved liquids and sinking of dense cumulates will promote convective stirring and mixing of liquids and crystals (Christiansen, 2005). This magma chamber is envisioned as the upper-crustal product of a distillation process involving differentiation at various depths (Fig. 13; Bachman and Bergantz, 2008; Lee and Morton, 2015).

Although the Wyoming batholith is chemically homogeneous, its initial Nd isotopic composition is not uniform. In the western end of the batholith, the initial Nd isotopic composition matches the Bears Ears pluton, suggesting that similar magma sources supplied the Louis Lake batholith and western Wyoming batholith. The less radiogenic ε_{Nd} of the batholith exposed in the

Shirley and Laramie Mountains requires a higher proportion of Archean crustal sources or involvement of a less radiogenic crustal source. This isotopic variability implies that although vertical stirring was effective, the batholith is less well-homogenized horizontally. Moreover, it suggests that the batholith was supplied by multiple conduits that tapped intermediate magma chambers of varying Nd isotopic composition (Fig. 13).

The characteristics of the large silicic batholiths associated with continental arcs have been inferred from the compositional and temporal record of their voluminous ignimbrite products (Christiansen, 2005; de Silva and Gosnold, 2007), and in the case of the Altiplano-Puna volcanic field, from the seismic evidence of the magma system beneath (Ward et al., 2014). We interpret the Wyoming batholith as an exposed example of one of these batholiths, and as such it provides an important opportunity for direct study of the processes producing large volumes of siliceous magma.

As noted above, potassic granites are a common component of every Archean craton, and are the second most widespread lithology in Neoarchean terranes after the tonalite-trondhjemite-granodiorite association (Laurent et al., 2014). Like the Wyoming batholith, these Neoarchean granites, which have high silica contents (typically 70-76% SiO_2), are not associated with intermediate and mafic phases (Laurent et al., 2014). Extensive areas composed exclusively of granite are notable feature of Neoarchean terrains. For example, the Turfloop and Lekkersmaak biotite granites dominate the southern Pietersburg block of the Kaapvaal province (Laurent et al., 2014). Individual granite suites in the Slave Province occupy fully 60% of a 130 km x 110 km map sheet (Davis et al., 1994) and together they extend across the entire craton (Davis and Bleeker, 1999). Neoarchean potassic granite occupies 20% of the area of the Yilgarn craton, and is distributed throughout the entire craton (Cassidy et al., 2006). The formation of these granites seems to require a large power input from the mantle applied across a broad area. Slab breakoff, retreat, and/or lithospheric delamination have been proposed to expose the base of the crust to heat from the mantle that ultimately is responsible for extensive granite magmatism (Laurent et al., 2014; Davis and Bleeker, 1999; Davis et al., 1994). The late

Archean Earth may present optimal conditions for the formation of large volumes of silicic magma. By this time the majority of the planet's continental crust had formed (e.g. Hawkesworth et al., 2010), providing the environment in which differentiation, distillation, and assimilation could occur. In addition, the Earth's internal radioactive heat production was still relatively high, providing the power to drive these processes.

Acknowledgements

This project was supported by NSF grant EAR9909260 and by the U.S. Geological Survey EDMAP program. DAB acknowledges a research assistantship from the University of Wyoming School of Energy Resources. We thank B.R. Frost, S.M. Swapp, and J.F. McLaughlin for stimulating discussions and C.W. Nye for assistance with figures.

References Cited

Ague, J.J., and Brimhall, G.H. (1988) Magmatic arc asymmetry and distribution of anomalous plutonic belts in the batholiths of California: Effects of assimilation, crustal thickness, and depth of crystallization. Geological Society of America Bulletin, 100, 912-927.

Bachmann, O., and Bergantz, G.W. (2008) Rhyolites and their source mushes across tectonic settings. Journal of Petrology, 49, 2277-2285.

Bachmann, O., Dungan, M.A., Lipman, P.W. (2002) The Fish Canyon magma body, San Juan volcanic field, Colorado: rejuvenation and eruption of an upper-crustal batholith. Journal of Petrology, 43, 1469-1503.

Bachmann, O., Deering, C.D., Lipman, P.W., and Plummer, C. (2014) Building zoned ignimbrites by recycling silicic cumulates: insight from the 1,000 km3 Carpenter Ridge Tuff, CO. Contributions to Mineralogy and Petrology, 167, 1025.

Bagdonas, D.A. (2014) Petrogenesis of the Neoarchean Wyoming batholith, central Wyoming. M.S.

thesis, University of Wyoming, Laramie, 120 pp.

Bateman, P. C., and Chappell, B. W. (1979) Crystallization, fractionation and solidification of the Tuolumne Intrusive series, Yosemite National Park, California. Geological Society of American Bulletin, 90. 465-482.

Best, M.G., Barr, D.L., Christiansen, E.H., Gromme, C.S., Deino, A.L., and Tingey, D.G. (2009) The Great Basin altiplano during the middle Cenozoic ignimbrite flareup: Insights from volcanic rocks. International Geology Review, 51, 589-633.

Best, M.G., Christiansen, E.H., and Gromme, S. (2013a) Introduction: the 36-18 Ma southern Great Basin, USA, ignimbrite province and flareup: swarms of subduction-related supervolcanoes. Geosphere, 9, 260-274.

Best, M.G., Christiansen, E.H., Deino, A.L., Gromme, S., Hart., G.L., and Tingey, D.G. (2013b) The 36-18 Ma Indian Peak-Caliente ignimbrite field and calderas, southeastern Great Basin, USA: Multicyclic super-eruptions. Geosphere, 9, 864-950.

Black, L.P., Kamo, S.L., Allen, C.M., Aleinikoff, J.N., Davis, D.W., Korsch, R.J., and Foudoulis C. (2003) TEMORA 1: a new zircon standard for Phanerozoic U–Pb geochronology. Chemical Geology, 200, 155–170.

Bowers, N.E., and Chamberlain, K.R. (2006) Precambrian history of the Eastern Ferris Mountains and Bear Mountain, central Wyoming province. Canadian Journal of Earth Sciences, 43, 1467-1487.

Cassidy, K.F., Champion, D.C., and Smithies, R.H. (2006) Origin of Archean late potassic granites: evidence from the Yilgarn and Pilbara cratons. Geochimica et Cosmochimica Acta, 70.18S, A88.

Chamberlain, K.R., Frost, C.D., and Frost, B.R. (2003) Early Archean to Mesoproterozoic evolution of the Wyoming province: Archean origins to modern lithospheric architecture. Canadian Journal of Earth Sciences, 40, 1357-1374.

Charlier, B.L.A., Bachmann, O., Davidson, J.P., Dungan, M.A., and Morgan, D.J. (2007) The upper crustal evolution of a large silicic magma body; evidence from crystal-scale Rb-Sr isotopic heterogeneities in the Fish Canyon magmatic system, Colorado. Journal of Petrology, 48, 1875-1894.

Christiansen, E.H. (2005) Contrasting processes in silicic magma chambers: evidence from very large volume ignimbrites. Geological Magazine,142, 669-681.

Christiansen, E.H., and Best, M.G. (2014) Constraints on the origin of subduction-related ignimbrite flareups from source volume calculations; the southern Great Basin ignimbrite province. Geological Society of America Abstracts with Programs, 46, 374.

Condie, K.C. (1969) Petrology and geochemistry of the Laramie batholith and related metamorphic rocks of Precambrian age, eastern Wyoming. Geological Society of America Bulletin, 80, 57-82.

Davis, W.J. and Bleeker, W. (1999) Timing of plutonism, deformation, and metamorphism in the Yellowknife Domain, Slave Province, Canada. Canadian Journal of Earth Sciences, 36, 1169-1187.

Davis, W.J., Fryer, B.J., and King, J.E. (1994) Geochemistry and evolution of Late Archean plutonism and its significance to the tectonic development of the Slave craton. Precambrian Research, 67, 207-241.

DePaolo, D.J., Perry, F.V., Baldridge, W.S. (1992) Crustal versus mantle sources of granitic magmas: a two-parameter model based on Nd isotopic studies. Transactions of the Royal Society of Edinburgh: Earth Sciences, 83, 439-446.

De Silva, S.L., Zandt, G., Trumbull, R., Viramonte, J.G., Salas, G., Jimenez, N. (2006) Large ignimbrite eruptions and volcano-tectonic depressions in the Central Andes: a thermomechanical perspective. In C. Troise, G. de Natale, and C.R.J. Kilburn, Eds., Mechanisms of activity and unrest at large caldera. Geological Society of London Special

Publications, 47–63.

De Silva, S.L., and Gosnold, W.D. (1995) Episodic construction of batholiths: insights from the spatiotemporal development of an ignimbrite flare-up. Journal of Volcanology and Geothermal Research, 167, 320-335.

De Silva, S.L., and Wolff, J.A. (2007) Zoned magma chamber; the influence of magma chamber geometry on sidewall convective fractionation. Journal of Volcanology and Geothermal Research, 65, 111-118.

Folkes, C.B., de Silva, S.L., Wright, H.M., and Cas, R.A.F. (2011) Geochemical homogeneity of a long-lived, large silicic system; evidence from the Cerro Galán caldera, NW Argentina. Bulletin of Volcanology, 73, 1455-1486.

Frost, B.R., and Frost, C.D. (2014) Essentials of Igneous and Metamorphic Petrology, Cambridge University Press, 303 p.

Frost, B.R., Frost, C.D., Hulsebosch, T.P., Swapp, S.M. (2000) Origin of the charnockites of the Louis Lake Batholith, Wind River Range, Wyoming. Journal of Petrology, 41, 1759-1776.

Frost, B.R., Arculus, R.J., Barnes, C.G., Collins, W.J., Ellis, D.J., and Frost, C.D. (2001) A geochemical classification of granitic rocks. Journal of Petrology, 42, 2033-2048.

Frost, B.R., and Frost, C.D. (2008) A geochemical classification for feldspathic igneous rocks. Journal of Petrology, 49, 1955-1969.

Frost, C.D. and Fanning, C.M. (2006) Archean geochronological framework of the Bighorn Mountains, Wyoming. Canadian Journal of Earth Sciences, 43, 1399-1418.

Frost, C.D., Frost, B.R., and Beard, J.S. (2016) On silica-rich granitoids and their eruptive equivalents. American Mineralogist, doi:10.2138/am-2015-5307.

Frost, C.D., Frost, B.R., McLaughlin, J.F., Swapp, S.M., Fanning, C.M. (2015) Formation of Paleoarchean Continental Crust in the central Wyoming Province. Geological Society of America Abstracts with Programs, 47(7), 721.

Frost, C.D., Frost, B.R., Chamberlain, K.R., and Hulsebosch, T.P. (1998) The Late Archean history of the Wyoming province as recorded by granite plutonism in the Wind River Range, Wyoming. Precambrian Research, 89, 145-173.

Frost, C.D., Fruchey, B.L., Chamberlain, K.R., Frost, B.R. (2006) Archean crustal growth by lateral accretion of juvenile supracrustal belts in the south-central Wyoming province. Canadian Journal of Earth Sciences, 43, 1533-1555.

Fruchey, B.L. (2002) Archean supracrustal sequences of contrasting origin: the Archean history of the Barlow Gap area, northern Granite Mountains, Wyoming. M.S. thesis, University of Wyoming, Laramie. 178 p.

Hawkesworth, C.J., Dhuime, B., Pietranik, A.B., Cawood, P.A., Kemp, A.I.S., and Storey, C.D. (2010) The generation and evolution of the continental crust. Journal of the Geological Society of London, 167, 229-248.

Jaguin, J., Gapais, D., Poujol, M., Boulvais, P., and Moyen, J.-F. (2012) The Murchison greenstone belt (South Africa): a general tectonic framework. South African Journal of Geology, 115, 65-76.

Kay, S.M., Mpodozis, C., Coira, B. (1999) Neogene magmatism,tectonism, and mineral deposits of the central Andes (22° to 33°S latitude). In B.J. Skinner, R. Holland, Eds., Geology and Ore Deposits of the Central Andes. Society of Economic Geologists Special Publications, 27–59.

Kay, S.M., Coira, B.L., Caffe, P.J., Chen, C. –H. (2010) Regional chemical diversity, crustal andmantle sources and evolution of central Andean Puna plateau ignimbrites. Journal of Volcanology and Geothermal Research, 198, 81-111.

Langstaff, G.D. (1995) Archean geology of the Granite Mountains, Wyoming. Ph.D. dissertation, Colorado School of Mines, Golden.

Laurent, O., Martin, H., Moyen, J.F., and Doucelance, R. (2014) The diversity and evolution of late-Archean granitoids: evidence for the onset of “modern-style” plate tectonics between 3.0 and

2.5 Ga. Lithos, 205, 208-235.

Lee, C-T. A., Morton, D.M., Kistler, R.W., Baird, A.K. (2007) Petrology and tectonics of Phanerozoic continent formation: from island arcs to accretion and continental arc magmatism. Earth and Planetary Science Letters, 263, 370-387.

Lee, C-T. A., and Morton, D.M. (2015) High silica granites: terminal porosity and crystal settling in shallow magma chambers. Earth and Planetary Science Letters, 409, 23-31.

Lindsay, J.M., de Silva, S., Trumbull, R., Emmermann, R., Wemmer, K. (2001). La Pacana Caldera, N. Chile; a re-evaluation of the stratigraphy and volcanology of one of the world’s largest resurgent calderas. Journal of Volcanology and Geothermal Research, 106, 145-173.

Lipman, P.W. (2007) Incremental assembly and prolonged consolidation of Cordilleran magma chambers: evidence from the Southern Rocky Mountain volcanic field. Geosphere, 3, 42-70.

Lipman, P.W. and Bachmann, O. (2015) Ignimbrites to batholiths: integrating perspectives from geological, geophysical, and geochronological data. Geosphere, 11, 705-743.

Love, J.D. (1970) Cenozoic geology of the Granite Mountains area, central Wyoming. U.S. Geological Survey Professional Paper 495-C, 154 p.

Ludwig. K.R. (2001) SQUID 1.02, A User's Manual. Berkeley Geochronology Center Special Publication, Berkeley, CA, USA.

Ludwig. K.R. (2003) User's Manual for Isoplot/Ex, Version 3.0, A Geochronology Toolkit for Microsoft Excel. Berkeley Geochronology Center Special Publication, Berkeley, CA, USA.

Ludwig, K.R., and Stuckless, J.S. (1978) Uranium-lead isotope systematics and apparent ages of zircons and other minerals in Precambrian granitic rocks, Granite Mountains, Wyoming. Contributions to Mineralogy and Petrology, 65, 243-254.

Maughan, L.L., Christiansen, E.H., Best, M.G., Gromme, C.S., Deino, A.L., and Tingey, D.G. (2002) The Oligocene Lund Tuff, Great Basin, USA; a very large volume monotonous intermediate. Journal of Volcanology and Geothermal Research, 113, 129-157.

McLaughlin, J.F., Bagdonas, D., Frost, C.D., Frost, B.R. (2013) Geologic Map of the Stampede Meadows quadrangle, Fremont County, Wyoming. Wyoming State Geological Survey Bedrock Geologic Map, 1:24,000 scale, 1 sheet.

Meredith, M.T. (2005) A Late Archean tectonic boundary exposed at Tin Cup Mountain, Granite Mountains, Wyoming. M.S. thesis, University of Wyoming, Laramie.

Mogk, D.W., Mueller, P.A., Wooden, J.L. (1988) Tectonic aspects of Archean continental development in the North Snowy Block, Beartooth Mountains, Montana. Journal of Geology, 96, 125-141.

Mogk, D.W., Mueller, P.A., Wooden, J.L. (1992) The significance of Archean terrane boundaries: evidence from the northern Wyoming province. Precambrian Research, 55, 155-168.

Moyen, J.-F. (2011) The composite Archean grey gneisses: petrological significance, and evidence for a non-unique tectonic setting for Archaean crustal growth. Lithos, 123, 21-36.

Mueller, P.A., and Frost, C.D. (2006) The Wyoming province: a distinctive Archean craton in Laurentian North America. Canadian Journal of Earth Sciences, 43, 1391-1397.

Mueller, P.A., Shuster, R., Wooden, J., Erslev, E., Bowes, D. (1993) Age and composition of Archean crystalline rocks from the southern Madison Range: implications for crustal evolution in the Wyoming craton. Geological Society of America Bulletin, 105, 437-446.

Mueller, P.A., Wooden, J.L., Mogk, D.W., Nutman, A.P., Williams, I.S. (1996) Extended history of a 3.5 Ga trondhjemitic gneiss, Wyoming province, USA: evidence from U-Pb systematics in zircon. Precambrian Research, 78, 41-52.

Mueller, P., Wooden, J., Nutman, A., Mogk, D. (1998) Early Archean crust in the northern Wyoming province: evidence from U-Pb systematics in detrital zircons. Precambrian Research, 91, 295-307.

Mueller, P., Wooden, J., Heatherington, A., Burger, H., Mogk, D., D'Arcy, K. (2004) Age and evolution of the Precambrian crust of the Tobacco Root Mountains. In: Brady, J.B., Burger, H.R., Cheney, J.T., and Harms, T.A., eds. Precambrian geology of the Tobacco Root Mountains, Montana. Geological Society of America Special Paper, 377, 181-202.

Pearce, J.A., Harris, N.B.W., and Tindle, A.G. (1984) Trace element discrimination diagrams for the tectonic interpretation of granitic rocks. Journal of Petrology, 25, 956-983.

Peterman, Z.E., and Hildreth, R.A. (1978) Reconnaissance geology and geochronology of the Precambrian of the Granite Mountains, Wyoming. U.S. Geological Survey Professional Paper, 1055, 22 p.

Putirka, K.D., Canchola, J., Rash, J., Smith, O., Torrez, G., Paterson, S.R., and Ducea, M.H. (2014) Pluton assembly and the genesis of granitic magmas: insights from the GIC pluton in cross section, Sierra Nevada Batholith, California. American Mineralogist, 99, 1284-1303.

Robbins, S.L., and Grow, J.A. (1992) Implications of Gravity and seismic reflection data for Laramide mountain ranges and basins of Wyoming and southern Montana. U.S. Geological Survey Bulletin 2012-E, 20 p.

Ross, K.T., Christiansen, E.H., Best, M.G., Dorais, M.J. (2015) Cooling before super-eruption: no evidence of rejuvenation in a crystal-rich dacite magma body, southern Great Basin ignimbrite province, Utah and Nevada. American Geophysical Union Fall Meeting abstract V13B-3125

Souders, A.K. and Frost, C.D. (2006) In suspect terrane? Provenance of the Late Archean Phantom Lake Metamorphic Suite, Sierra Madre, Wyoming. Canadian Journal of Earth Sciences, 43, 1557-1577.

Stuckless, J.S. (1989) Petrogenesis of Two Contrasting Late Archean Granitoids, Wind River Range, Wyoming. U.S. Geological Survey Professional Paper, 1491, 38p.

Stuckless, J.S., and Peterman, Z.E. (1977) A summary of the geology, geochronology, and geochemistry of Archean rocks of the Granite Mountains, Wyoming. Wyoming Geological Association, Earth Science Bulletin, 10.3, 3-20.

Stuckless, J.S., Bunker, C.M., Busg, C.A., Doering, W.P., and Scott, J.H. (1977). Geochemical and petrologic studies of a uraniferous granite from the Granite Mountains, Wyoming. U.S. Geological Survey Journal of Research, 5, 61-81.

Stuckless, J.S. and Miesch, A.T. (1981) Petrogenetic Modeling of a Potential Uranium Source Rock, Granite Mountains, Wyoming. U.S. Geological Survey Professional Paper, 1224, 34p.

Stuckless, J.S., Hedge, C.E., Worl, R.G., Simmons, K.R., Nkomo, I.T., and Wenner, D.R. (1985) Isotopic studies of the late Archean plutonic rocks of the Wind River Range, Wyoming. Geological Society of America Bulletin, 96, 850-860.

Sutherland, W.M., and Luhr, S.C. (2011) Preliminary bedrock geologic map of the Farson 30' x 60' Quadrangle, Sweetwater, Sublette, and Fremont Counties, Wyoming. Wyoming State Geological Survey Open File Report WSGS-2011-OFR-06, scale 1:100,000, 1 sheet.

Wall, E.N. (2004) Petrologic, geochemical and isotopic constraints on the origin of 2.6 Ga post-tectonic granitoids of the central Wyoming province. M.S. thesis, University of Wyoming, Laramie.

Ward, K.M., Zandt, G., Beck, S.L., Christiansen, D.H. (2014) Seismic imaging of the magmatic underpinnings beneath the Altiplano-Puna volcanic complex from the joint inversion of surface wave dispersion and receiver functions. Earth and Planetary Science Letters, 404, 43-53.

Williams, I.S. (1998) U-Th-Pb geochronology by ion microprobe. Reviews in Economic Geology, 7, 1-35.

Figure Captions

Figure 1. Location of the Wyoming province and subprovinces, and the project area of this investigation (blue dashed line).

Figure 2. Map of central Wyoming showing extent of Archean outcrop, including 2.62-2.63 Ga granitic rocks of the Wyoming batholith and Louis Lake batholith. The largest of the other ~2.62 Ga

granites is the Bears Ears pluton, which intrudes the Louis Lake batholith. Laramide basement-involved thrust faults brought the Archean rocks to the present-day erosional surface. Subsequent Cenozoic normal faulting down-dropped the Granite and Shirley Mountains a minimum of 700 meters (Love, 1970).

Figure 3. Field photographs of Wyoming batholith rocks. (a) Lankin Dome, central Granite Mountains, is composed of biotite granite at the base and is capped by leucocratic banded granite. The contact is sharp along the west end (red arrow) and feathered in the center and east end (black arrow) of Lankin Dome. The summit is at 2354m, 420 m above the valley floor. (b) View of the southern face of Lankin Dome taken from the base of the outcrop. The boundary between leucocratic banded granite (top) and the biotite granite (bottom) is interfingered (note people below the shadowed horizontal ledge in central-left of image for scale). (c) Contact between leucocratic banded and biotite granites as viewed from near the contact on the southern face of Lankin Dome. The foreground shows the coarse texture of the leucocratic banded granite. The black arrow indicates the scalloped nature of the boundary with the biotite granite. (d) Unnamed peak in the central Granite Mountains near Sweetwater Station, showing incorporation of leucocratic banded granite within biotite granite. The large, folded enclave of leucocratic banded granite is interpreted to have detached from the batholith roof and been deformed during magmatic flow along with other smaller and wispy inclusions of the leucocratic banded granite.

Figure 4. Photomicrographs of biotite granite samples 11SMG2, 13SM05, and 12GM04 are shown in images a, b, and c. (a) Quartz has undergone deformation and grain-boundary migration. Plagioclase is weakly sericitized. Epidote and chlorite are secondary after biotite. (b) Microcline is perthitic. Biotite commonly contains inclusions of zircon and magnetite. Although not visible in the photomicrograph, rutile needles are common as inclusions within quartz. (c) Finer-grained biotite granite sample showing serated grain boundaries formed by

subsolidus grain boundary migration. Potassium feldspar may also have undergone high temperature grain-size reduction. Photomicrographs of leucocratic banded granite samples 12SMG9, 13LR02, and 12SMG3 are shown in images d, e, and f. (d) Graphic granite texture is fairly common, as shown in this photomicrograph. (e) Plagioclase is sericitized and biotite has undergone deuteric alteration. Magnetite is associated with biotite. (f) Grain-size of quartz and feldspars varies widely in leucocratic banded granite samples; this photomicrograph is dominated by a large quartz crystal. A small crystal of muscovite is present in the upper part of the photomicrograph.

Figure 5. (a) Concordia diagram for zircon from leucocratic banded granite sample 10LD2. The $^{207}Pb/^{206}Pb$ age of the concordant analysis, 2627 ± 3 Ma (1σ), is interpreted as the best estimate for the age of this sample. (b) Concordia diagram for zircon from biotite granite sample 11SMG1. 5 analyses of zircon with U < 600 ppm define a mean weighted age of 2623 ± 4.3 Ma (1σ), which is interpreted as the best estimate of the crystallization age of this sample. (c) Concordia diagram for zircon from hydrothermally altered biotite granite sample 11SMG2. The two grains with the lowest uranium contents are shown in red. The most concordant analysis (-1% discordant) yielded a $^{207}Pb/^{206}Pb$ age of 2624 ± 4 Ma (1σ), which is interpreted as the best estimate for the age of this sample.

Figure 6. Plots of (a) Fe index [$FeO^{tot}/(FeO^{tot} + MgO)$], (b) modified alkali-lime index (MALI; $Na_2O + K_2O – CaO$), and (c) aluminum saturation index (ASI; molecular ratio Al/Ca – 1.67P + Na + K) for the Wyoming and Louis Lake batholiths. The Wyoming batholith has a restricted range of silica, and is mainly magnesian, calc-alkalic to alkali-calcic, and peraluminous. No geochemical variations by geographic location are apparent. By contrast, the Louis Lake batholith includes intermediate to mafic components and is calc-alkalic and metaluminous. Data from Table 1; Condie, 1969; Stuckless and Peterman, 1977; Stuckless and Miesch, 1981; Frost et al., 1998;

Frost et al., 2000; Wall, 2004; and Meredith, 2005. Boundaries of fields are from Frost et al. (2001) and Frost and Frost (2008).

Figure 7. Variation diagrams of SiO_2 versus (a) K_2O, (b) Rb, (c) Sr, and (d) Eu. Incompatible elements K and Rb increase modestly with silica in the Louis Lake batholith. Wyoming batholith and high silica granites of the Louis Lake batholith are high-K. They exhibit a four- to five-fold range in K_2O and Rb indicating that potassium feldspar and biotite are late-crystallizing phases. Compatible elements Sr and Eu show the opposite trends, and very low contents in the Wyoming batholith and high-silica components of the Louis Lake batholith. Symbols and data sources as in Fig. 7.

Figure 8. Diagrams of (a) Nb versus Y, and (b) Nb + Y versus Rb for samples of Wyoming and Louis Lake batholith rocks, after Pearce et al. (1984). Most samples are within the volcanic arc granite (VAG) field. Cumulate hornblende likely contributes to higher Nb and Y in Louis Lake batholith samples. COLG = collisional granites, ORG = ocean ridge granites, WPG = within plate granites. Symbols as in Fig. 7. Data from Table 1; Frost et al., 1998; Frost et al., 2000; and Wall, 2004.

Figure 9. Chondrite-normalized rare earth element diagrams for Wyoming batholith samples from the Granite Mountains (a), Shirley Mountains (b), and Laramie Mountains (c). Rare earth patterns for the Louis Lake batholith and Bears Ears pluton of the Wind River Range are shown in (d). Data sources: Table 1; Frost et al., 1998; and Stuckless, 1989.

Figure 10. Initial ε_{Nd} of Wyoming batholith samples compared to Louis Lake batholith and Bears Ears pluton samples. All samples were intruded at ~2.62-2.63 Ga; the Louis Lake and Bears Ears are displaced to the left of their intrusive age for clarity. Also shown are potential magma sources, including depleted mantle, ~3.3-3.4 Ga crust of the Sacawee block immediately north of the Wyoming batholith in the Granite Mountains, evolved metasedimentary rocks of the Granite Mountains, and juvenile metasediments of the southern accreted terranes in the Wind River

(DOI will not work until issue is live.) DOI: http://dx.doi.org/10.2138/am-2016-5512

Range and Granite Mountains. The Wyoming batholith in the Shirley and Laramie Mountains contains less radiogenic Nd isotopic ratios, suggesting that these magmas incorporated a greater proportion of old crust than the granites of the Granite Mountains and Wind River Range. Data sources: Table 2, Frost et al., 2006; Fruchey, 2002; Wall, 2004; and Meredith, 2005.

Figure 11. Nd isotopic compositions and locations within the Wyoming batholith. Nd isotopic compositions are grouped into three categories: red circles = samples with initial $_{Nd}$ < -3.4; pink circles = samples with intermediate values of $_{Nd}$ between -3.4 and -1.0; yellow circles = samples with initial $_{Nd}$ > -1.0. Data from Table 2 and Wall, 2004.

Figure 12. Plot of K_2O versus silica comparing the Wyoming batholith with eruptive products of Cerro Galán caldera, northwest Argentina (Folkes et al., 2011). The small black dots represent analyses of ignimbrite glass and the field encompasses compositions of pumice clasts. Data sources as in Fig. 7 and Folkes et al., 2011.

Figure 13. Schematic east-west cross-section through the central Wyoming province in the Neoarchean, depicting relative depth of emplacement of the Wyoming batholith and the Louis Lake/Bears Ears composite batholith. The Louis Lake batholith, which was emplaced at 3-6 kb (Frost et al., 2000), intrudes juvenile accreted terranes along its southern boundary. Nd isotopic evidence suggests that similar magma sources supplied the Louis Lake batholith and western Wyoming batholith but a larger proportion of evolved Archean crustal sources contributed to the eastern part of the Wyoming batholith. BEP = Bears Ears pluton.

This is a preprint, the final version is subject to change, of the American Mineralogist (MSA)
Cite as Authors (Year) Title. American Mineralogist, in press.
(DOI will not work until issue is live.) DOI: http://dx.doi.org/10.2138/am-2016-5512

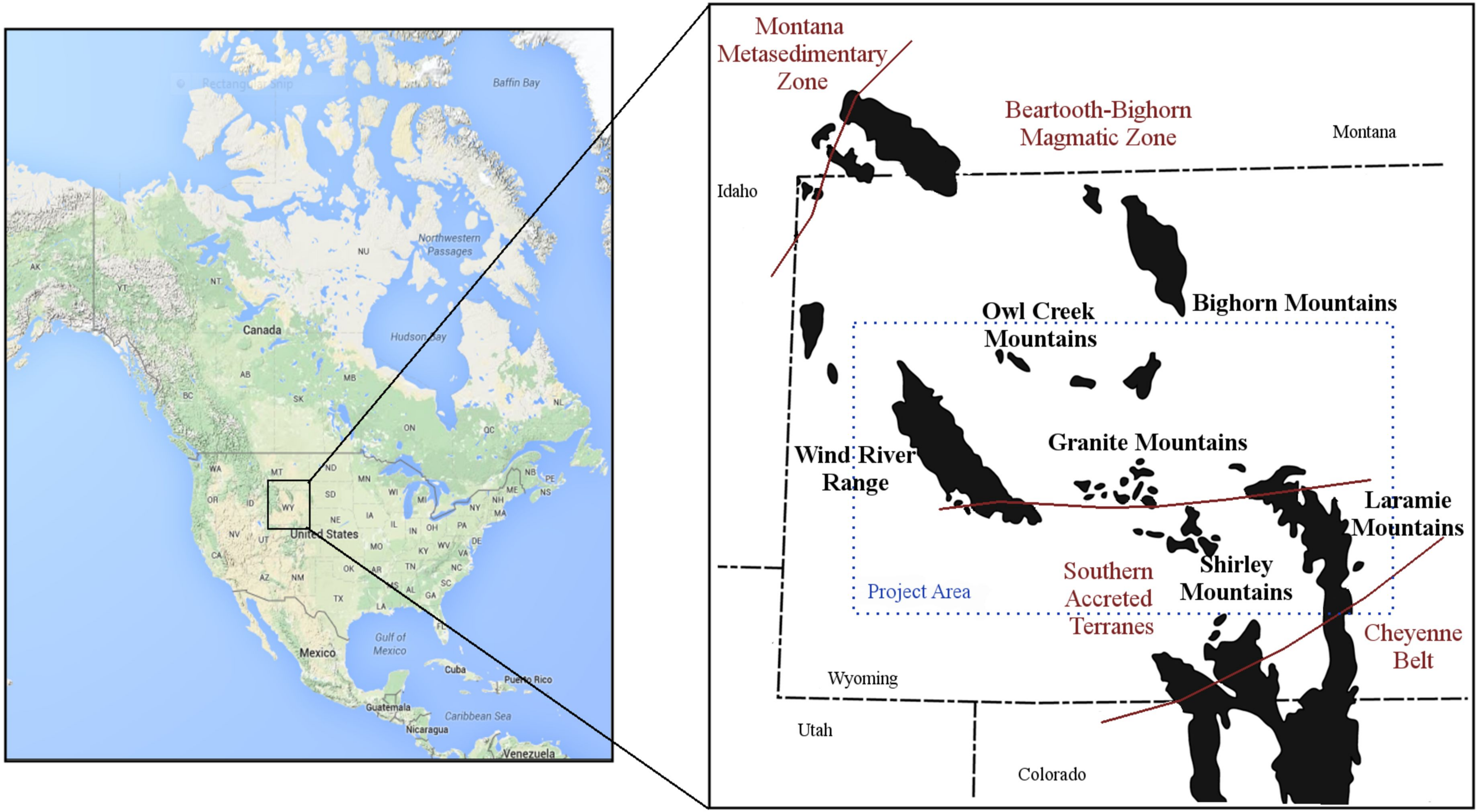

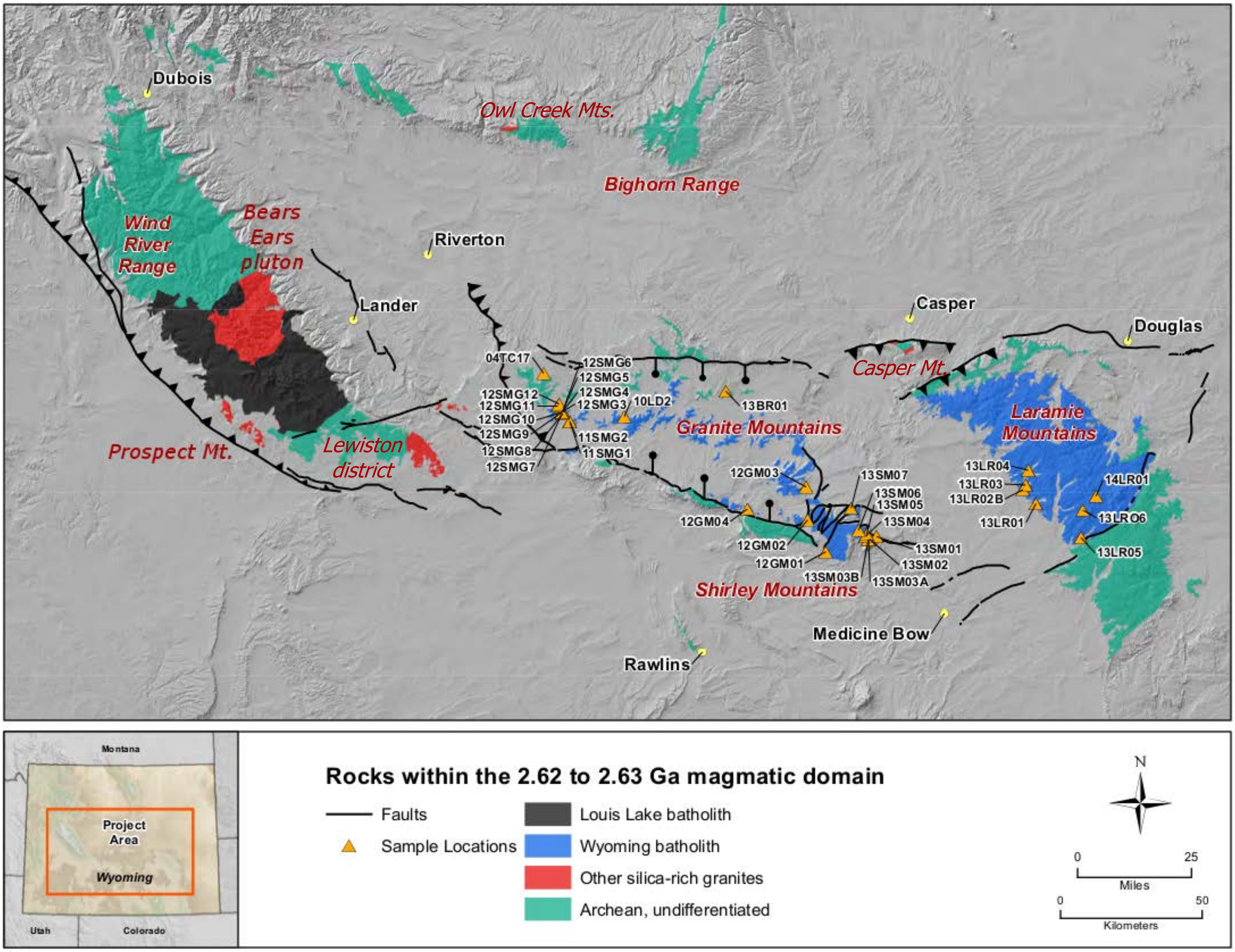
Dubois
Owl Creek Mts.
Bighorn Range
Wind River Range
Bears Ears pluton
Riverton
Lander
Casper
Douglas
Casper Mt.
Laramie Mountains
Granite Mountains
Prospect Mt.
Lewiston district
Shirley Mountains
Medicine Bow
Rawlins
04TC17
12SMG6
12SMG5
12SMG4
12SMG3
12SMG12
12SMG11
12SMG10
12SMG9
12SMG8
12SMG7
11SMG2
11SMG1
10LD2
13BR01
12GM03
12GM04
12GM02
12GM01
13SM07
13SM06
13SM05
13SM04
13SM01
13SM02
13SM03B
13SM03A
13LR04
13LR03
13LR02B
13LR01
14LR01
13LR06
13LR05
Montana
Project Area
Wyoming
Utah
Colorado
Rocks within the 2.62 to 2.63 Ga magmatic domain
Faults
Sample Locations
Louis Lake batholith
Wyoming batholith
Other silica-rich granites
Archean, undifferentiated
N
0 25 Miles
0 50 Kilometers

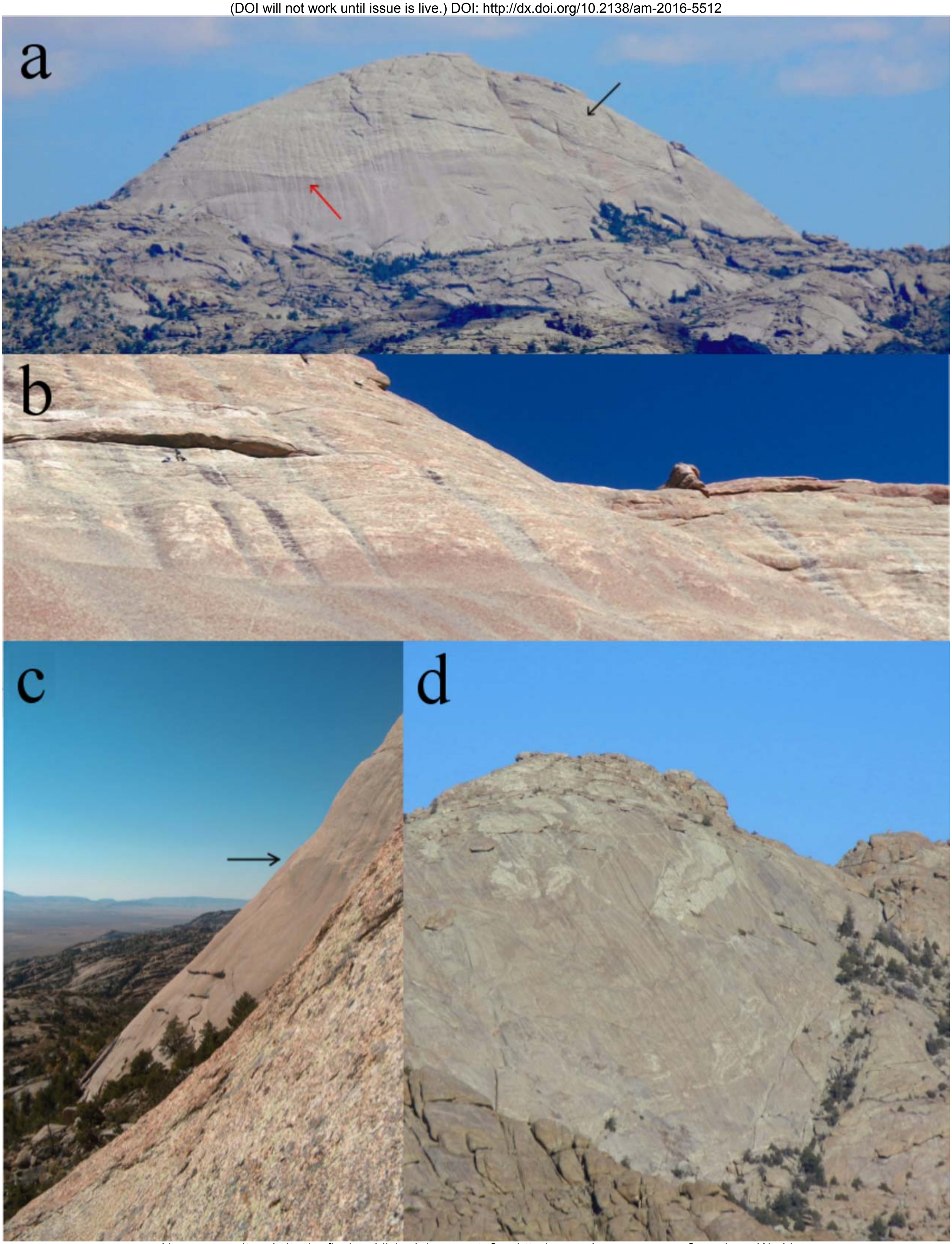
a
b
c
d

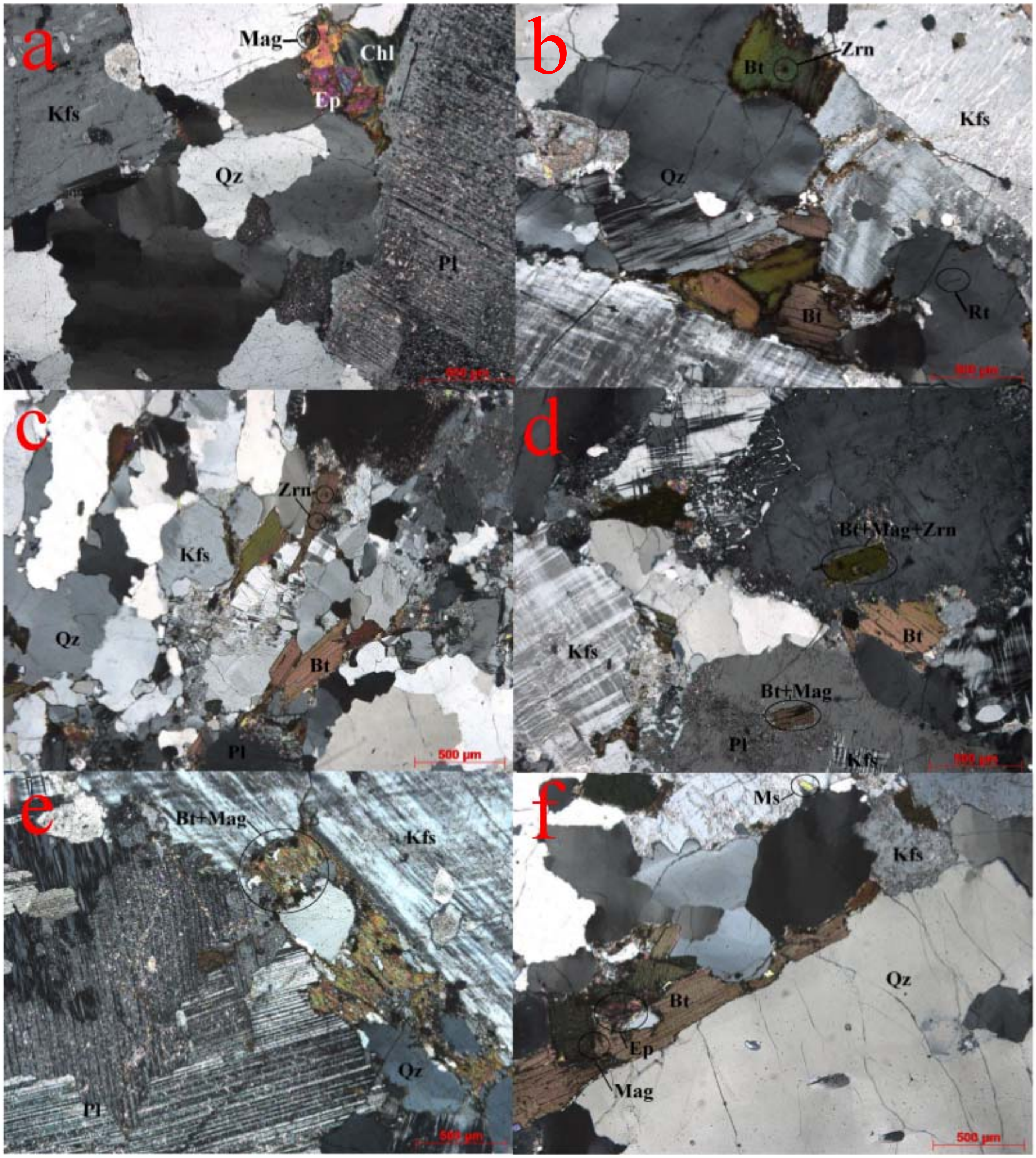
a
Mag
Chl
Ep
Kfs
Qz
Pl
b
Bt
Zrn
Kfs
Qz
Bt
Rt
c
Zrn
Kfs
Qz
Bt
Pl
500 μm
d
Bt+Mag+Zrn
Kfs
Bt
Bt+Mag
Pl
Kfs
e
Bt+Mag
Kfs
Qz
Pl
f
Ms
Kfs
Qz
Bt
Ep
Mag
500 μm

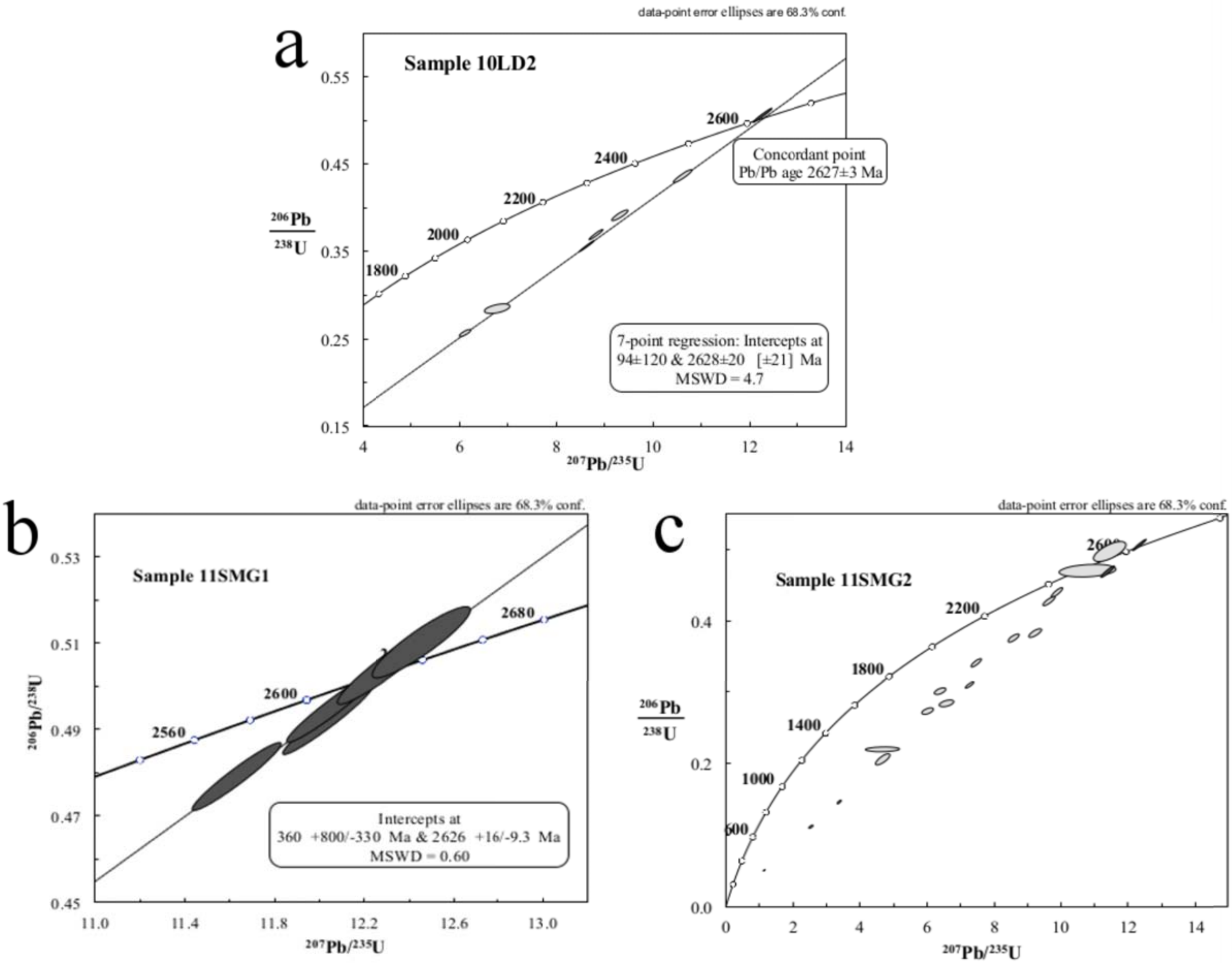
a
data-point error ellipses are 68.3% conf.
Sample 10LD2
1800
2000
2200
2400
2600
Concordant point
Pb/Pb age 2627±3 Ma
7-point regression: Intercepts at
94±120 & 2628±20 [±21] Ma
MSWD = 4.7
0.55
0.45
0.35
0.25
0.15
4
6
8
10
12
14
206Pb/238U
207Pb/235U
b
data-point error ellipses are 68.3% conf.
Sample 11SMG1
2560
2600
2680
Intercepts at
360 +800/-330 Ma & 2626 +16/-9.3 Ma
MSWD = 0.60
0.53
0.51
0.49
0.47
0.45
11.0
11.4
11.8
12.2
12.6
13.0
206Pb/238U
207Pb/235U
c
data-point error ellipses are 68.3% conf.
Sample 11SMG2
600
1000
1400
1800
2200
0.4
0.2
0.0
0
2
4
6
8
10
12
14
206Pb/238U
207Pb/235U

This is a preprint, the final version is subject to change, of the American Mineralogist (MSA)
Cite as Authors (Year) Title. American Mineralogist, in press.
(DOI will not work until issue is live.) DOI: http://dx.doi.org/10.2138/am-2016-5512

Figure 7

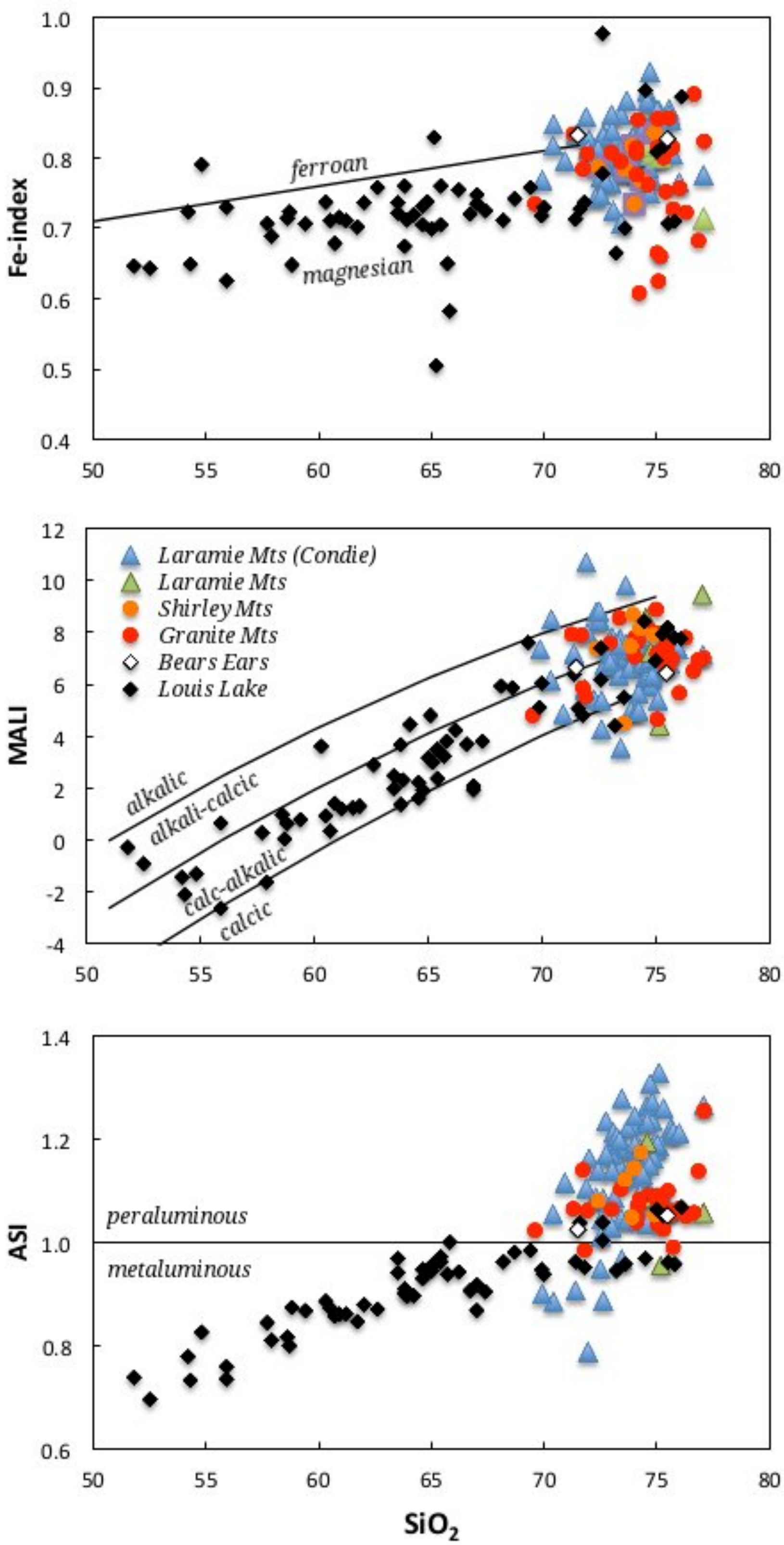

Figure 8

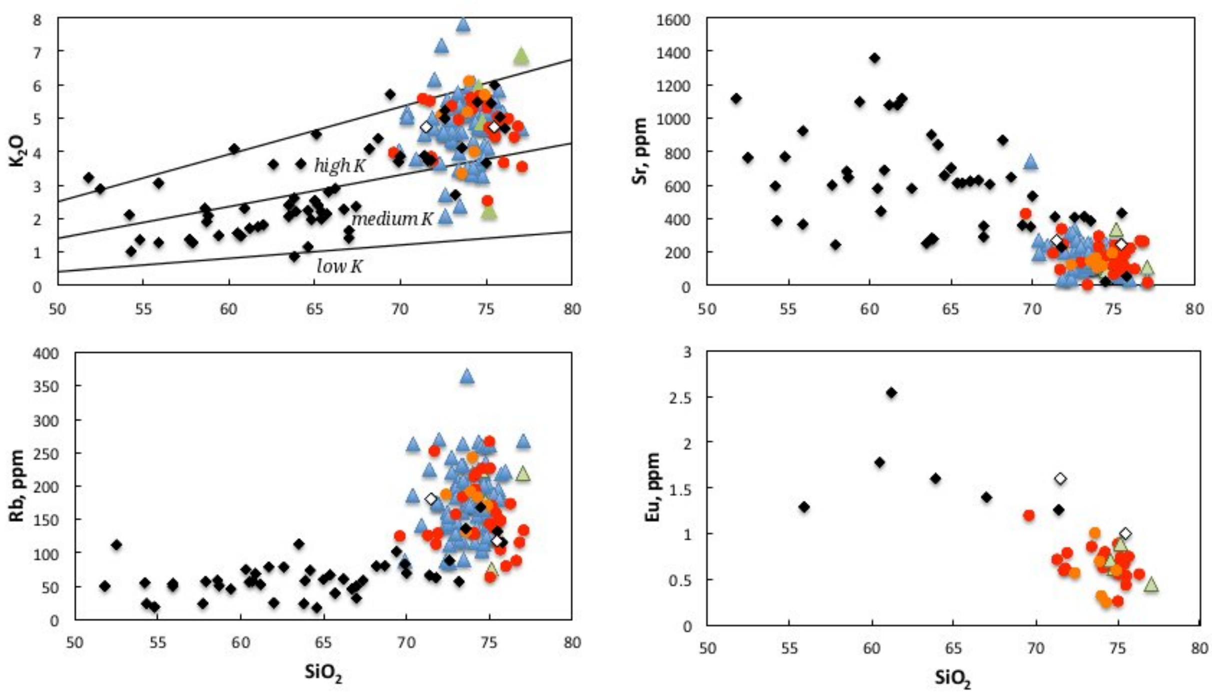

Figure 9

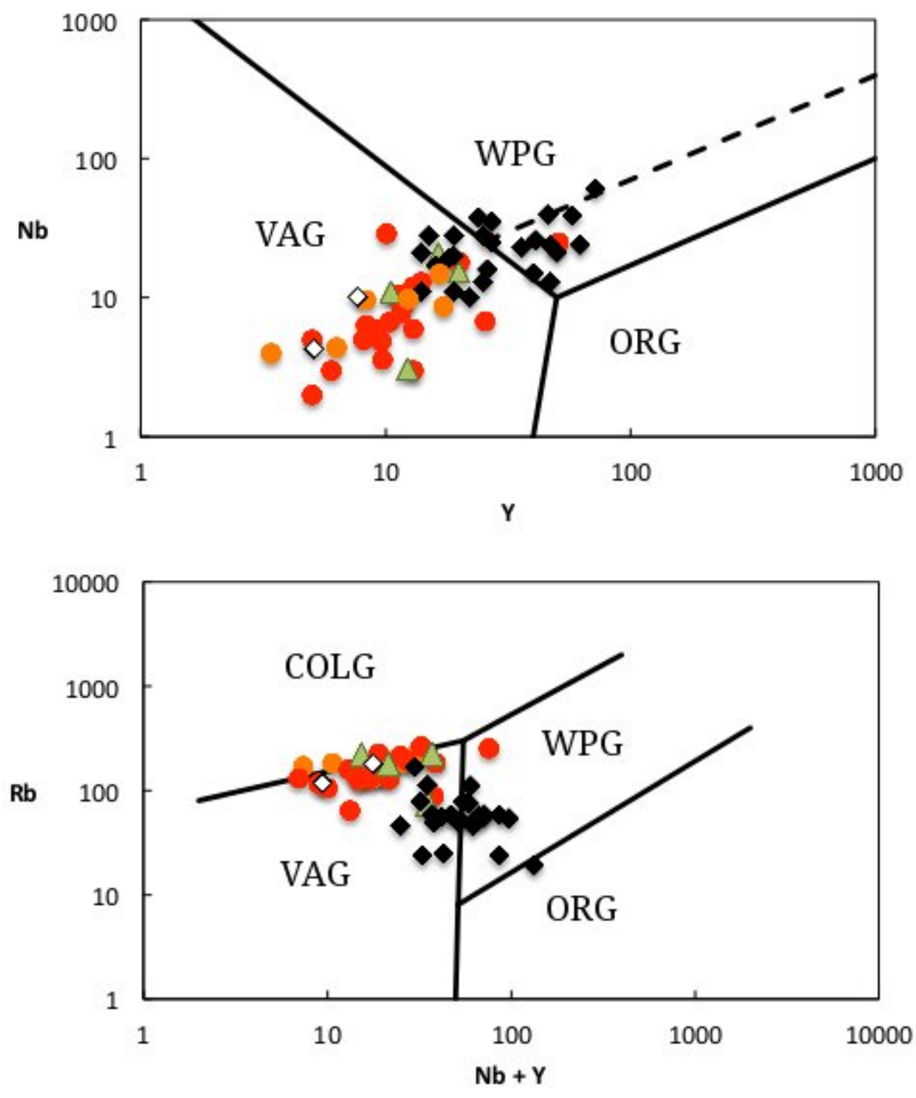
1000
100
10
1
Nb
WPG
VAG
ORG
1
10
100
1000
Y
10000
1000
100
10
1
Rb
COLG
WPG
VAG
ORG
1
10
100
1000
10000
Nb + Y

This is a preprint, the final version is subject to change, of the American Mineralogist (MSA)
Cite as Authors (Year) Title. American Mineralogist, in press.
(DOI will not work until issue is live.) DOI: http://dx.doi.org/10.2138/am-2016-5512

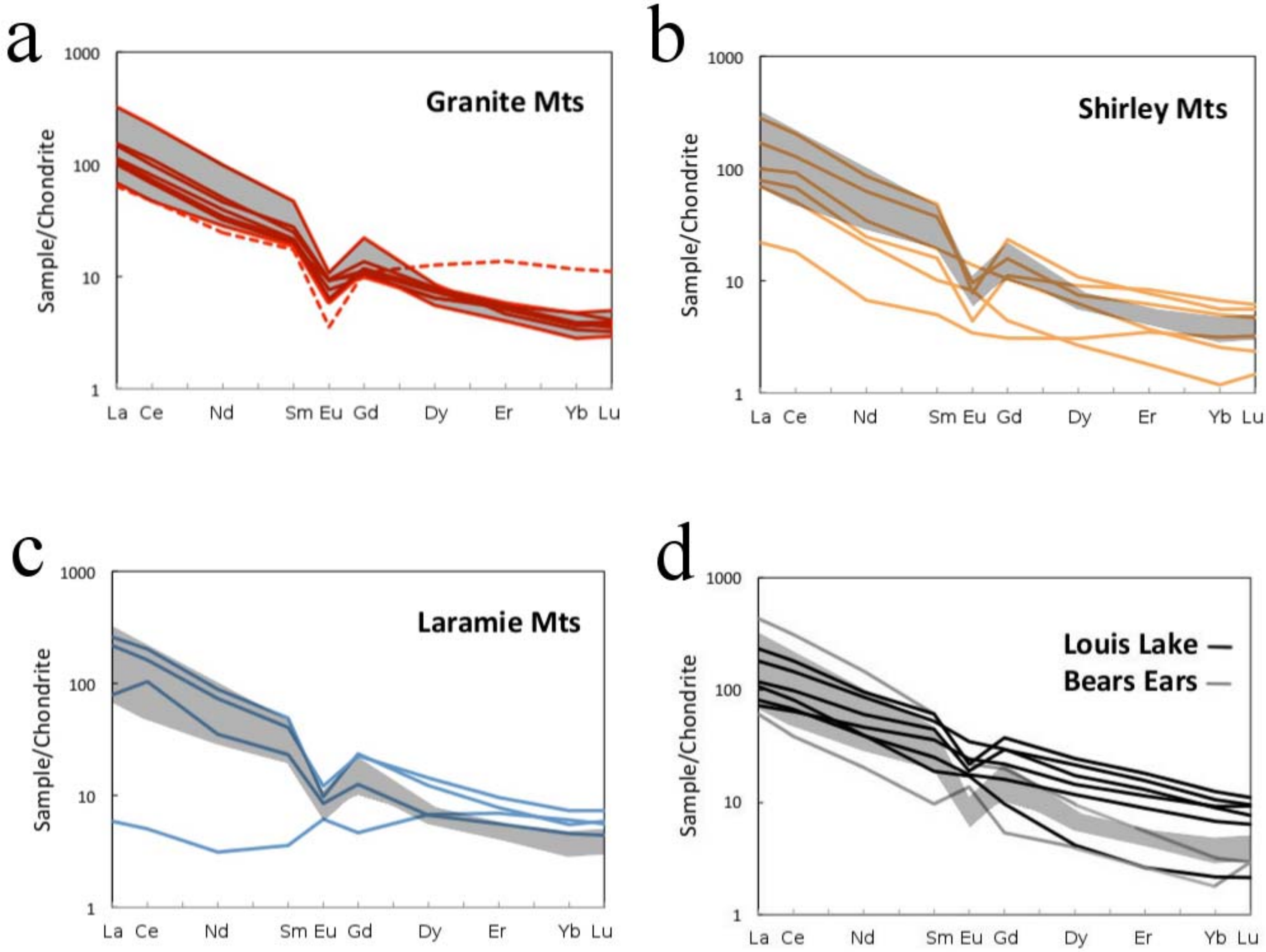

Figure 11

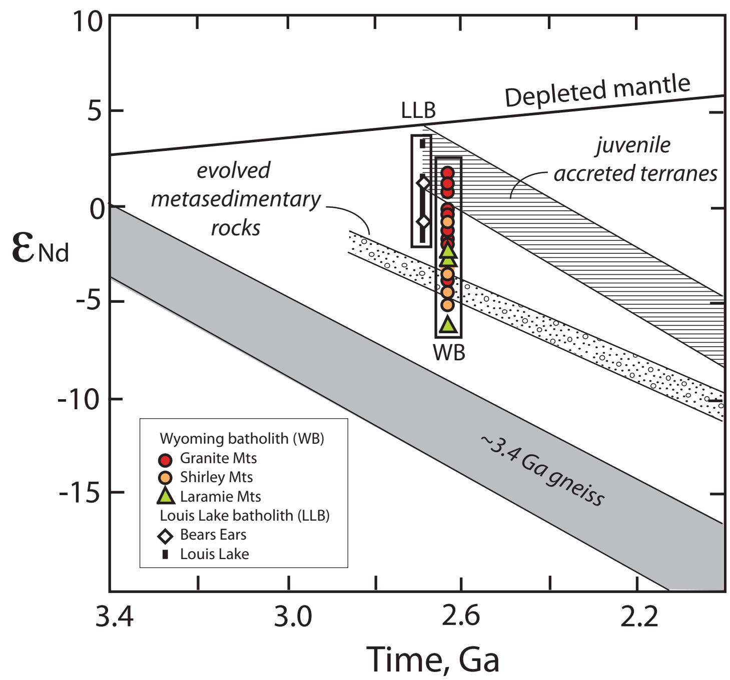
10
5
0
-5
-10
-15
εNd
3.4
3.0
2.6
2.2
Time, Ga
Depleted mantle
LLB
WB
juvenile
accreted terranes
evolved
metasedimentary
rocks
~3.4 Ga gneiss
Wyoming batholith (WB)
Granite Mts
Shirley Mts
Laramie Mts
Louis Lake batholith (LLB)
Bears Ears
Louis Lake

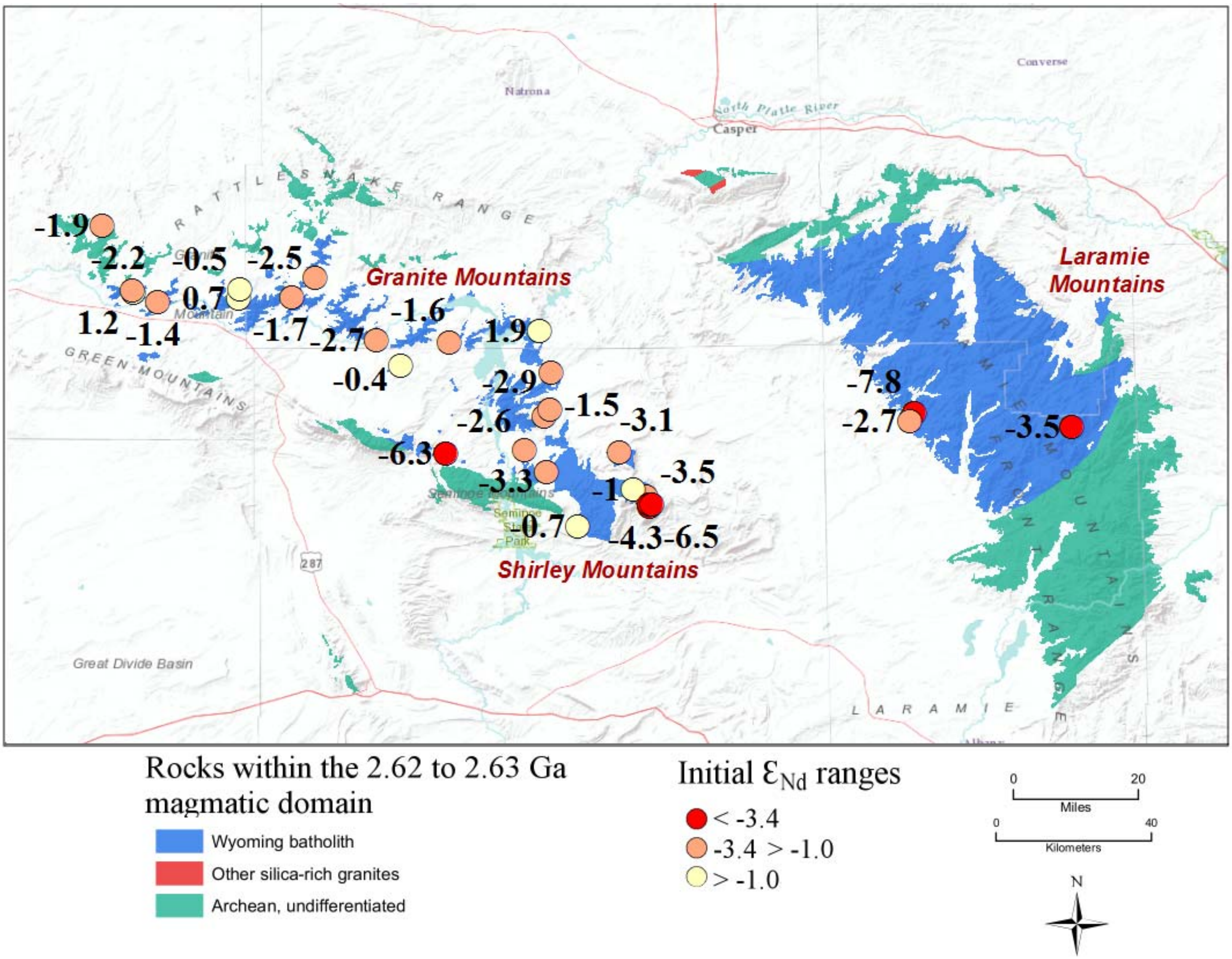
Natrona
Converse
North Platte River
Casper
RATTLESNAKE RANGE
Granite Mountains
Laramie Mountains
GREEN MOUNTAINS
Shirley Mountains
LARAMIE MOUNTAINS
LARAMIE
Great Divide Basin
287
-1.9
-2.2
-0.5
-2.5
0.7
1.2
-1.4
-1.7
-2.7
-1.6
1.9
-0.4
-2.9
-1.5
-2.6
-3.1
-6.3
-3.3
-3.5
-0.7
-4.3-6.5
-7.8
-2.7
-3.5
Rocks within the 2.62 to 2.63 Ga magmatic domain
Wyoming batholith
Other silica-rich granites
Archean, undifferentiated
Initial ε_{Nd} ranges
< -3.4
-3.4 > -1.0
> -1.0
0 20 Miles
0 40 Kilometers
N

Figure 12

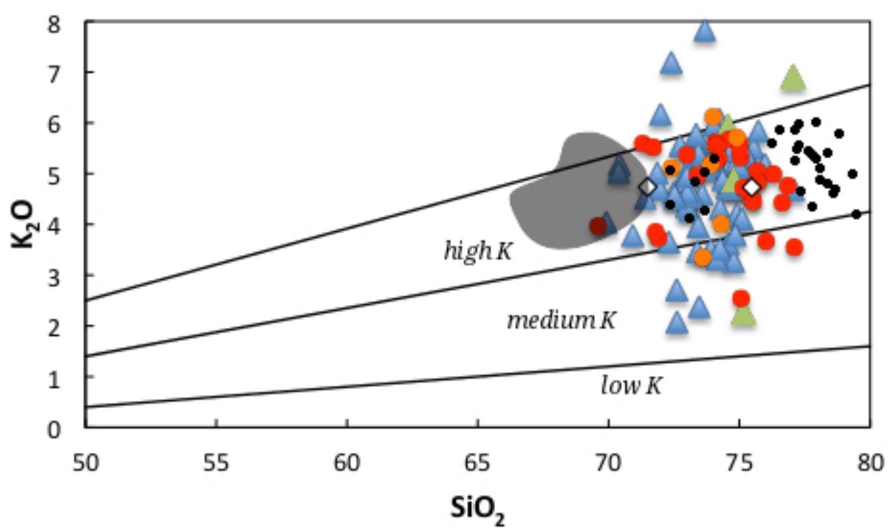

This is a preprint, the final version is subject to change, of the American Mineralogist (MSA)
Cite as Authors (Year) Title. American Mineralogist, in press.
(DOI will not work until issue is live.) DOI: http://dx.doi.org/10.2138/am-2016-5512

Figure 13

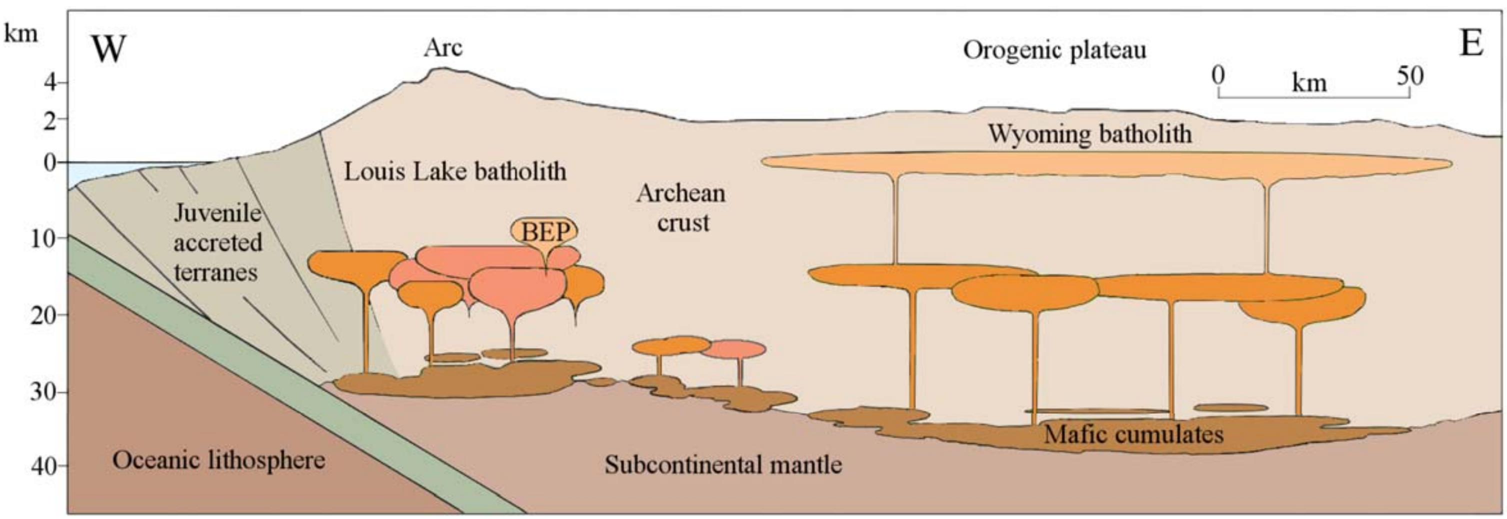

Table 1. Geochemistry of Neoarchean granite of the Wyoming batholith

	Granite Mountains									Shirley Mountains							Laramie Mountains			
	10LD-2	11SMG1	11SMG2	12SMG7	12GM01	12GM02	12GM03	12SMG9	04TC17*	12GM04	13SM02	13SM05	13SM06	13SM07	13SM03B	13SM03A	13LR01	13LR03	13LR02B	13LR06
SiO_2	75.02	75.07	72.99	71.30	76.30	71.91	75.40	74.10	75.50	75.30	73.60	73.90	74.90	72.40	74.00	74.30	77.70	74.70	73.50	73.50
TiO_2	0.06	0.26	0.24	0.09	0.16	0.37	0.08	0.10	0.10	0.12	0.32	0.18	0.11	0.17	0.14	0.14	0.03	0.15	0.22	0.18
Al_2O_3	14.58	14.41	13.67	14.55	13.45	14.40	12.90	14.45	13.75	14.05	13.60	14.45	13.45	14.20	13.70	14.55	12.95	13.80	13.40	13.75
$Fe_2O_3^{total}$	0.51	0.61	1.21	1.40	0.81	3.06	0.71	1.16	1.26	1.16	2.98	1.54	0.96	1.76	1.60	1.62	0.25	1.66	2.24	0.85
MnO	0.00	0.01	0.02	0.01	0.02	0.02	0.01	0.01	0.02	0.01	0.03	0.02	0.01	0.02	0.03	0.02	0.01	0.03	0.02	0.01
MgO	0.23	0.33	0.26	0.25	0.28	0.66	0.21	0.30	0.26	0.26	0.74	0.31	0.17	0.43	0.52	0.44	0.09	0.36	0.45	0.19
CaO	0.59	2.17	0.98	1.10	0.81	1.95	0.73	1.36	0.82	1.46	1.95	1.29	0.87	1.13	0.33	0.37	0.13	1.04	0.22	2.50
Na_2O	3.88	4.27	3.20	3.45	3.62	3.75	3.48	3.33	3.80	3.68	3.10	3.60	3.06	3.42	2.92	4.52	2.77	3.40	2.74	4.55
K_2O	5.60	2.54	5.37	5.59	4.99	3.73	4.74	5.62	4.48	4.65	3.35	5.18	5.71	5.11	6.12	4.01	6.91	4.88	5.93	2.27
P_2O_5	0.04	0.07	0.07	0.05	0.02	0.15	0.04	0.10	0.07	0.03	0.12	0.07	0.02	0.05	0.04	0.04	0.02	0.04	0.08	0.07
Total	100.52	99.73	98.01	97.79	100.46	100.00	98.30	100.53	100.06	100.72	99.79	100.54	99.26	98.69	99.40	100.01	100.61	98.40	96.56	97.02
Fe-index	0.66	0.62	0.81	0.83	0.72	0.81	0.75	0.78	0.81	0.80	0.78	0.82	0.84	0.79	0.73	0.77	0.7142857	0.8058252	0.8175182	0.8010471
MALI	8.89	4.65	7.60	7.94	7.80	5.53	7.49	7.59	7.46	6.87	4.50	7.49	7.90	7.40	8.71	8.16	9.4709178	7.2476825	8.5720662	4.4178555
ASI	1.08	1.05	1.06	1.06	1.05	1.06	1.06	1.04	1.10	1.03	1.12	1.05	1.05	1.08	1.14	1.17	1.0575032	1.0853025	1.193487	0.9548466
Rb ppm	266.4	64	157.5	126.5	174	129.5	160	128	144.5	136	132	191.5	171	187.5	243	183	219	177	223	75.6
Sr ppm	65.9	240.2	137.9	192.5	99.4	246	130.5	233	89.1	191	142.5	166.5	193.5	124	106	115.5	107.5	142.5	87.1	335
Zr ppm	64.8	143.4	141	85	93	306	112	105	89	108	194	156	58	175	118	124	107.5	142.5	87.1	335
Y ppm	25.5	9.7	9.6	8.3	11.1	11.3	8.1	10.4	11.6	11.9	8.3	12.4	3.4	17.2	16.6	6.3	12.3	10.5	16.4	19.9
Nb ppm	6.8	3.6	4.9	6.4	10.3	10.6	5	6.7	7.8	9	9.6	9.8	4	8.7	14.9	4.4	3.1	11	20.8	15.4
La ppm	21.6			46.1	38.6	110.5	52.4	23.2	35.2	50.0	33.6	57.3	23.5	95.2	26.7	7.5	2.0	26.9	87.8	73.8
Ce ppm	43.2			93.2	72.7	204.0	100.5	42.7	63.9	89.3	83.2	116.0	46.2	185.5	61.8	16.5	4.6	94.1	184.5	147.5
Pr ppm	4.5			10.5	7.6	18.9	10.1	5.2	6.4	8.9	6.3	11.9	4.3	16.9	4.7	1.3	0.4	6.4	17.7	14.7
Nd ppm	15.7			37.3	25.3	62.7	32.3	18.1	21.2	29.5	21.9	40.1	13.8	54.8	15.7	4.3	2.0	22.6	56.5	47.0
Sm ppm	3.4			7.3	4.2	9.1	4.9	3.6	4.0	5.4	3.8	7.2	2.0	9.4	3.1	1.0	0.7	4.5	9.5	7.9
Eu ppm	0.3			0.7	0.6	0.8	0.7	0.7	0.4	0.7	1.0	0.7	0.6	0.6	0.3	0.3	0.5	0.6	0.7	0.9
Gd ppm	2.8			4.7	2.6	5.7	2.9	2.7	3.0	3.6	2.7	4.1	1.2	6.1	2.9	0.8	1.2	3.3	6.1	5.9
Tb ppm	0.5			0.5	0.3	0.6	0.3	0.4	0.4	0.5	0.4	0.5	0.2	0.8	0.4	0.2	0.3	0.4	0.8	0.8
Dy ppm	3.8			2.2	1.9	2.6	1.7	1.9	2.3	2.4	1.9	2.2	0.8	3.2	2.7	0.9	2.0	2.0	3.7	4.3
Ho ppm	0.8			0.3	0.4	0.4	0.3	0.4	0.4	0.4	0.4	0.4	0.1	0.6	0.6	0.2	0.5	0.4	0.6	0.8
Er ppm	2.7			0.7	1.1	0.9	0.8	1.0	1.1	1.2	0.7	1.2	0.4	1.5	1.7	0.7	1.4	1.1	1.6	1.9
Tm ppm	0.4			0.1	0.2	0.1	0.1	0.1	0.2	0.1	0.1	0.2	0.1	0.2	0.3	0.1	0.2	0.1	0.2	0.3
Yb ppm	2.6			0.4	1.1	0.7	0.6	0.8	0.8	1.0	0.6	1.1	0.3	1.2	1.5	0.7	1.3	1.0	1.2	1.6
Lu ppm	0.4			0.1	0.2	0.1	0.1	0.1	0.1	0.1	0.1	0.2	0.1	0.2	0.2	0.1	0.2	0.2	0.2	0.3

*major element and Rb, Sr, Zr, Y and Nb data from Meredith (2005)

Major and minor element data obtained by ICP-AES and REE data by ICP-MS at ALS Minerals.

Sample locations are shown on Fig. 1 and UTM provided in Bagdonas (2014).

Fe-index, MALI, and ASI defined in Frost et al. (2001)

Table 2. Sm-Nd isotopic data for the Wyoming batholith.

Sample	Uplift	Sm ppm	Nd ppm	$^{147}Sm/^{144}Nd$	$^{143}Nd/^{144}Nd$	$^{143}Nd/^{144}Nd$ at 2625 Ma	ε_{Nd} at 2625 Ma
04TC17	Granite Mountains	3.6643	19.8219	0.11175	0.51107	0.509135	-1.90
10LD2	Granite Mountains	2.9180	13.7863	0.12796	0.51148	0.509269	0.72
12GM01	Granite Mountains	3.9440	24.4931	0.09734	0.51088	0.509197	-0.70
12GM02	Granite Mountains	9.0222	60.7883	0.08971	0.51062	0.509064	-3.31
12GM03	Granite Mountains	4.2724	29.1711	0.08853	0.51070	0.509165	-1.32
12SMG7	Granite Mountains	7.0978	35.4693	0.12098	0.51139	0.509294	1.21
12SMG9	Granite Mountains	3.5159	17.4107	0.12208	0.51124	0.509122	-2.16
12GM04	Shirley Mountains	4.3180	24.4961	0.10655	0.51079	0.508944	-5.65
13SM02	Shirley Mountains	3.6425	20.9785	0.10495	0.51072	0.508900	-6.51
13SM03A	Shirley Mountains	0.8204	4.1118	0.12061	0.51114	0.509056	-3.45
13SM03B	Shirley Mountains	2.7920	14.8652	0.11354	0.51098	0.509011	-4.34
13SM05	Shirley Mountains	6.5575	39.3692	0.10068	0.51082	0.509073	-3.13
13SM06	Shirley Mountains	2.1609	14.9477	0.08738	0.51069	0.509179	-1.04
13SM07	Shirley Mountains	5.1969	31.4543	0.09987	0.51080	0.509074	-3.10
13LR02B	Laramie Mountains	9.5015	57.1816	0.10044	0.51083	0.509094	-2.71
13LR03	Laramie Mountains	4.5403	22.6236	0.12131	0.51094	0.508837	-7.75
14LR1/LR94-7	Laramie Mountains	7.71975	54.31734	0.085904355	0.5105583	0.509071	-3.17

Sm and Nd were isolated from whole rock powders using methods described in Frost et al. (2006). Isotopic ratios were obtained on a Neptune MC-ICP-MS at the University of Wyoming. Samples were normalized to $^{146}Nd/^{144}Nd = 0.7219$. La Jolla Nd analyzed after every five unknowns gave $^{143}Nd/^{144}Nd = 0.51185 \pm 0.000012$ (2 s.d.)